PERGAMON

Journal of Structural Geology 22 (2000) 1065–1086

JOURNAL OF STRUCTURAL GEOLOGY

www.elsevier.nl/locate/jstrugeo

Extensional failure and hydraulic valving at Minas da Panasqueira, Portugal: evidence from vein spatial distributions, displacements and geometries

K.A. Foxford[a,*,1], R. Nicholson[a], D.A. Polya[a], R.P.B. Hebblethwaite[b]

[a]*Department of Earth Sciences, The University of Manchester, Manchester M13 9PL, UK*
[b]*The Coach House, Blackwell Hall Lane, Latimer, Chesham, Buckinghamshire HP5 1TN, UK*

Received 23 August 1999; accepted 3 March 2000

Abstract

At Panasqueira, Portugal, exceptional exposure and demonstrable vein connectivity allow robust characterisation of brittle/elastic failure mechanisms in intrusive-related environments. Extensional failure was driven by cycles of fluid injection (hydraulic valving) and vein growth under conditions with $\lambda_v \geq 1$ and differential stress $< 4T$. Failure was episodic and produced a swarm of W–Sn-bearing quartz veins characterised by positive volumetric strain. Worked veins consist of families of co-planar vein-lobes linked at branch-points. Geometrically coherent vein displacements constrain an elliptical anomaly (the damage zone) in which values of extensional strain are symmetrically distributed, decreasing systematically away from a centrally located maxima to zero at a tip-line loop. Vein textures indicate rapid, episodic, vein opening, μm- to dm-scale vein apertures, spatially and temporally variable rates of vein filling and periodic baffling of fluid migration pathways. Although the vein swarm represents a single vein cluster, vein thickness and spacing populations are typically non-power law and define anomaly-scale heterogeneous strain with inhomogeneously deformed marginal zones surrounding a homogeneously deformed high-strain core. Deviations from power-law behaviour were promoted by competitive vein growth that provided mechanisms for (i) inhibiting vein nucleation and (ii) localising deformation onto a few evenly spaced veins.

1. Introduction

At outcrop, evidence for hydraulic failure is manifest as swarms of extensional structures such as veins, igneous dykes and sills, or barren joints mantled by oxidised, reduced or otherwise altered wall rocks. Such fracture systems exhibit dual behaviour providing (1) a highly permeable migration pathway for large volumes of crustal fluids, e.g. hydrothermal solutions (aqueous or hydrocarbon) and magmas, and (2) pore space in which a reservoir of fluid is stored. Rapid fluid transport over substantial distances can potentially transfer heat and juxtapose fluids from substantially different sources. It may also result in significant fluid–rock disequilibrium, which can result in important geological effects such as degradation or enhancement of wall-rock porosity and permeability and precipitation of economic minerals. In consequence, extensional structures often retain material infillings and/or wall-rock alteration halos that provide important visual markers promoting reconstruction of extensional failure mechanisms and fluid flow histories.

Fluid overpressures develop when migrating fluids are impounded behind low permeability flow baffles (seals) such as lithological contacts, regions of cementation, or sealing portions of faults. Importantly, seals enable accumulation of pore pressures sufficient to produce conditions of effective tensile stress and to initiate extensional failure when:

* Corresponding author.
E-mail address: afoxford@middevon.gov.uk (K.A. Foxford).
[1] Present address: Consultant Geologist, Castle Farm, Huntsham, Tiverton, Devon EX16 7QH, UK.

0191-8141/00/$ - see front matter
PII: S0191-8141(00)00029-8

$$P_f = \sigma_3 + T_s \quad (1)$$

where (P_f) is the pore pressure, σ_3 is the least compressive stress, T_s is the fracture toughness of the seal or the cohesive strength of the critical pre-existing discontinuity, and values of differential stress $(\sigma_1-\sigma_3) \leq 4T$ (cf. Jaeger, 1963; Secor, 1965). If differential stresses exceed $4T$, fracture opening is mixed mode, i.e. accommodated by extensional and shear displacements (Price and Cosgrove, 1990, pp. 33–34).

Pore pressure at depth in the Earth's crust is conveniently expressed by the pore-fluid factor:

$$\lambda_v = \frac{P_f}{\sigma_v} \quad (2)$$

where σ_v is the vertical stress or overburden pressure (Sibson, 1990). When fluid pressure is hydrostatic $\lambda_v \approx 0.4$ whilst when $\lambda_v \rightarrow 1$ near lithostatic P_f conditions prevail. In a compressive regime with $\sigma_3 = \sigma_v$, hydraulic fractures form when $\lambda_v > 1$ provided the rock mass retains a finite tensile strength. However, Lorentz et al. (1991) suggest that at moderate levels of differential stress ($>4T$) extensional failure can occur at lower fluid overpressures with $\lambda_v \rightarrow 1$ if the overpressured unit is effectively unconfined, i.e. effective mean stress $\underline{\sigma}' = (\underline{\sigma} - P_f) \rightarrow 0$, where $\underline{\sigma}$ is the mean stress (Cox and Etheridge, 1989). Under these conditions the dilatancy accompanying extensional failure is accommodated by a combination of pore pressure and interbedded anelastic strata whilst fracture apertures are supported over extended periods of time by compressive stress.

Constriction of a migration pathway, e.g. through crack-healing or a drop in pore pressure, often facilitates a cyclical process involving fluid impounding, P_f build-up, fracture reopening and episodic fluid expulsion (valving) along the established pathway. When extensional failure produces a pathway that neither exploits existing structural discontinuities nor accommodates significant shear strain, a characteristic type of brittle/elastic damage zone is propagated comprising an array of opening-mode veins that constitute a positive volumetric strain anomaly of simple sill- or dyke-like form. We refer to this end-member type of extensional failure as hydraulic-valving behaviour. The more common end-member is fault-valving behaviour (see Sibson et al., 1988; Sibson, 1990, 1994; Boullier and Robert, 1992; Cox et al., 1995) where extensional failure exploits structural weaknesses, such as faults, and involves residual or other shear strain resulting in more complex vein geometries and strain distributions.

Our understanding of extensional structures has been developed through four separate lines of study: (1) statistical analysis of fracture spacings, thicknesses and displacement geometries as determined from line transects through vein swarms (e.g. Sanderson et al., 1994; Vermilye and Scholz, 1995; Clark et al., 1995; Gillespie et al., 1999; Roberts et al., 1999); (2) textural analysis of vein material to define fracture opening/infilling histories (Grigorev, 1965; Ramsay, 1980; Ramsay and Huber, 1983; Cox and Etheridge, 1983; Halls, 1987; Nicholson, 1991; Foxford et al., 1991a, b); (3) serial sectioning to define vein geometry and connectivity (Nicholson and Pollard, 1985; Nicholson and Ejiofor, 1987; Foxford et al., 1995); and (4) experimentation and modelling work on fracture nucleation and growth processes, interactions and relationships with ambient stress fields (see reviews in Atkinson, 1987; Pollard and Aydin, 1988; Bahat, 1991, as well as Pollard, 1987; Rogers and Bird, 1987; Olson and Pollard, 1989, 1991; Hull, 1993; Wu and Pollard, 1993). However, spatial and temporal variability in vein geometry and accretion rates are best considered at the system-scale and in relation to failure mechanisms.

In this paper we determine the relationships in an intrusive-related environment between high pressure fluids, extensional strain and veining using a multidisciplinary approach. Our data are drawn from the sill-like swarm of well-characterised W–Sn-bearing quartz veins at Panasqueira, Portugal, where vein connectivity is demonstrable. We report spatial variations in vein distribution, displacements and geometry at the vein lobe- and damage zone-scales and integrate the results with textural data to constrain failure and fluid migration histories. The implications for the development of damage zones characterised by positive volumetric strain and produced through episodic valving of overpressured crustal fluids are then discussed. Our results are set in a fracture mechanics framework and broadly support the hypothesis of Sanderson et al. (1994) that some mineralised vein systems show departures from power law behaviour.

1.1. Growth and geometry of extensional veins

Damage zones comprising arrays of extensional veins can be modelled in profile view as systems of coplanar cracks (cf. Olson and Pollard, 1991; Renshaw and Pollard, 1994) that open parallel to σ_3 and propagate in the $\sigma_1-\sigma_2$ plane (Secor, 1965). Failure at elevated P_f can be geologically rapid, e.g. when overpressure is released by injection of excess fluid into hydraulic fractures in adjacent sealing units. The fractures propagate when tensile stresses exceeding the fracture toughness of the material are generated at crack tips (cf. Lawn and Wilshaw, 1975).

Our conceptual view of extensional vein morphology is given in Fig. 1. Only isolated veins in isotropic rocks can approach the ideal, unrestricted, penny shape. Once wall-rock heterogeneity and tip-line confinement processes are introduced vein shapes inevitably attain more complex lobed and bladed forms (Fig. 1b). Wall-rock heterogeneity induces differential rates of propa-

gation at vein tips resulting in vein segmentation through tip-line bifurcation, the resulting vein lobes being separated by thick wall-rock bridges (Nicholson and Ejiofor, 1987; Foxford et al., 1995). Similar tip-line differential growth mechanisms are used to explain the bladed geometries and propagation directions of cracks in ceramics (Hull, 1993), igneous dykes (Delaney and Pollard, 1981) and sills (Pollard et al., 1975), joints (Pollard et al., 1982; Pollard and Aydin, 1988; Bahat, 1997) and normal faults (Huggins et al., 1995; Childs et al., 1995; Nicol et al., 1996).

Lobed veins also result from tip-line confinement accompanying impingement and overlap of the stress fields at propagating but closely spaced lobe tip-lines (Pollard et al., 1982; Pollard and Aydin, 1988; Olson and Pollard, 1991). Often, both tip-line bifurcation and confinement processes operate together; vein lobes produced through tip-line bifurcation grow out of plane during continued propagation, impinge and overlap producing progressively more restricted and bladed geometries. As neighbouring vein lobes impinge, the overlap zones (bridges) are folded and flexed because it becomes energetically more favourable to flex bridges rather than to increase amounts of overlap by propagation. With continued lobe growth, bridges rupture and adjacent lobes become linked producing compound veins with stepped walls (Nicholson and Pollard, 1985).

Thickness balancing (Beach, 1975) is a necessary feature of geometrically coherent vein swarms characterised by positive volumetric strain since otherwise the host rock is required to deform in a manner inconsistent with brittle/elastic deformation. Vein thickness data, therefore, provide constraints on vein geometry, kinematics and scaling relationships. Foxford et al. (1995, figure 6B) demonstrate contoured vein thicknesses projected onto a map of the top-vein surface are systematically distributed, being at a maximum in vein centres and decreasing regularly and systematically towards vein edges. Contours are sub-elliptical and sub-parallel to the margin of the vein (Fig. 1c). Thickness profiles (plots of vein thickness against distance along the vein) are typically bell-shaped due to tip-line confinement (Foxford et al., 1995; Vermilye and Scholz, 1995), a feature which lead Peacock (1991) to liken vein thickness behaviour to that of the throw distribution on systems of normal faults (cf. Barnett et al., 1987; Walsh and Watterson, 1991; Childs et al.,

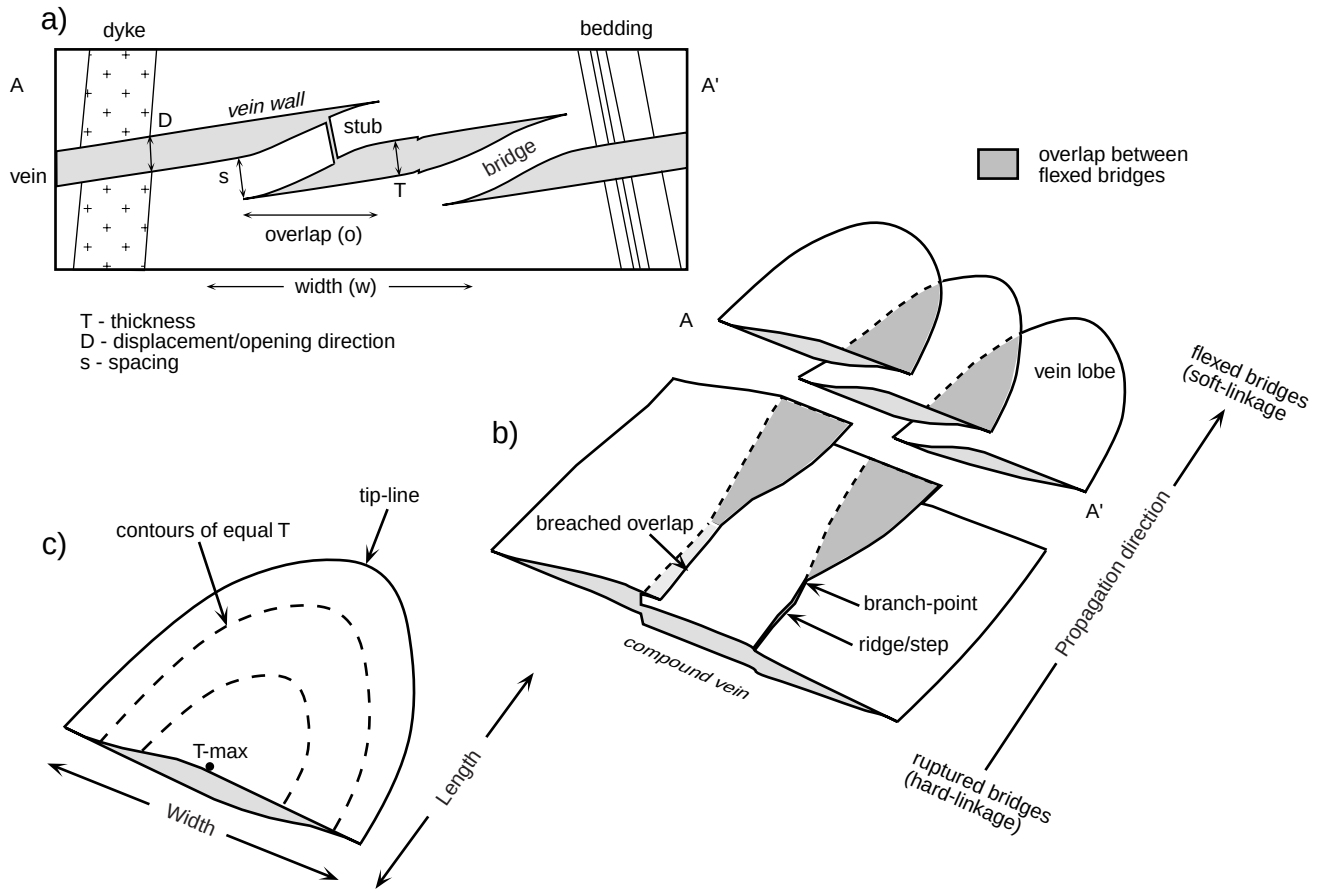

Fig. 1. Schematics illustrating nomenclature, morphology and displacement distributions for mode I veins. (a) Cross-section of compound vein. (b) Illustration of lobed and bladed vein geometry. (c) Thickness contours for a simple vein lobe.

1995). Similar displacement profiles have been reported from igneous dykes (Pollard and Segal, 1987).

Like overlap zone behaviour in fault systems (cf. Walsh and Watterson, 1991; Childs et al., 1995), bridges separating adjacent veins can be divided into those that show vein thickness transfer and those that do not. Veins separated by bridges across which aggregated vein thicknesses are balanced are kinematically interdependent in both two- and three dimensions, the stress fields at overlapping vein tips impinging during their growth aiding propagation and causing the vein thickness distribution on each to be influenced by the other. In contrast, bridges that are kinematically independent occur between veins either too widely separated to have interacted or that grew at different times.

1.2. Constraints on data collection

At Panasqueira, underground exploitation of W-bearing quartz veins dates from ca. 1912 (Smith, 1979) and has resulted in extensive delineation of the vein swarm. The essentially flat-lying veins are worked by means of longwall and, more recently, room and pillar stoping methods (Smith, 1979; Mello Mendes et al., 1987), the latter producing 2 km of accessible three-dimensional exposure per hectare of stope workings. Stopes are developed from a system of haulages laid out on a 100 m grid with five separate 60-m-thick intervals (levels) connected by vertical raises and spiral ramps. Historically, exploration has largely been from the inside outwards defining a well-characterised core zone, containing the thickest veins, surrounded by poorly constrained marginal zones whose numerous thin veins outcrop in the vicinity of the mine and facilitated its discovery. The plentiful subsurface exposure, demonstrable connectivity between stoped veins and numerous drillcore records provide data vastly more comprehensive than obtainable at natural surface outcrop. Vein thicknesses are available for all worked vein portions and exploratory drillcores; however, the mine operators employ an arbitrary vein thickness cut-off of veins >5 cm thickness when recording these data.

1.3. Analytical techniques

Vein spatial distributions, kinematics and geometry have been constrained by verifying stope and drillcore records with extensive mapping and measurement at the stope face. Vein opening histories have been deduced using stope face observations and slabbed and polished samples covering all structural locations within veins and all stages of the paragenesis. Polished thin sections (ca. 100) were made from selected samples and examined using standard microscopic techniques. Values of linear vertical strain have been derived by computer gridding, and then aggregating, vein thickness values for each mine level using ZMAP plus™ software. Despite the paucity of information for veins <5 cm threshold thickness, making our values of strain underestimates, the available data encompass all packets of veins of economic potential discovered to date.

2. The Panasqueira W–Sn-bearing quartz veins

2.1. Geological setting

Located about 34 km west of Fundão in the central Portuguese province of Beira Baixa (Fig. 2), Minas da Panasqueira exploits a sill-like damage zone consisting of sub-horizontal W–Sn-bearing quartz veins situated above a granitoid batholith, the Panasqueira granite, enclosed within a tightly folded complex of schists and psammites, the Xisto-grauvaquica das Beiras or Beira Schists (Thadeu, 1951), which have a NW–SE-aligned regional foliation. Regional greenschist metamorphism of the Beira Schist occurred during the early stages of the Hercynian Orogeny and was accompanied by the formation of tight, upright folds. Numerous pods and vein-like mass of deformed and recrystallised quartz (seixo bravo) probably also formed at this time (Thadeu, 1951; d'Orey, 1967). The granitic batholith forms part of the Hercynian granitic complex of northern Portugal and was emplaced into the Pre-Cambrian to Carboniferous age Beira Schists prior to veining (Kelly and Rye, 1979). The upper levels of the granite are

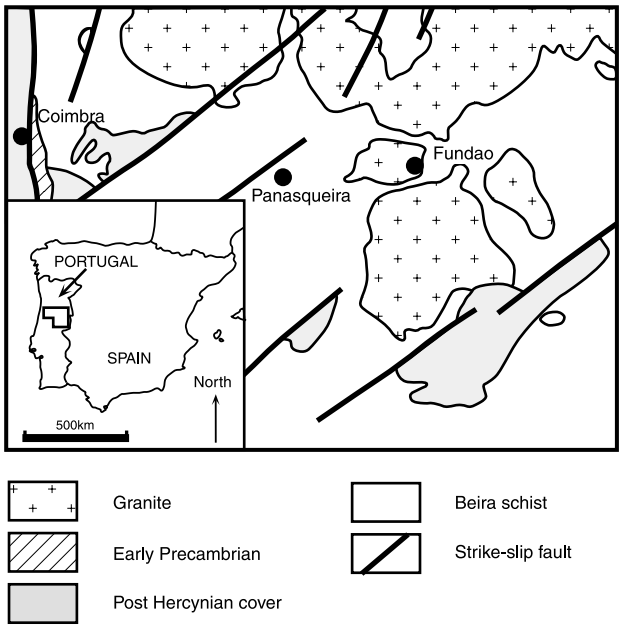

Fig. 2. Location and geological setting of the study area (redrawn after Inverno and Ribeiro, 1980).

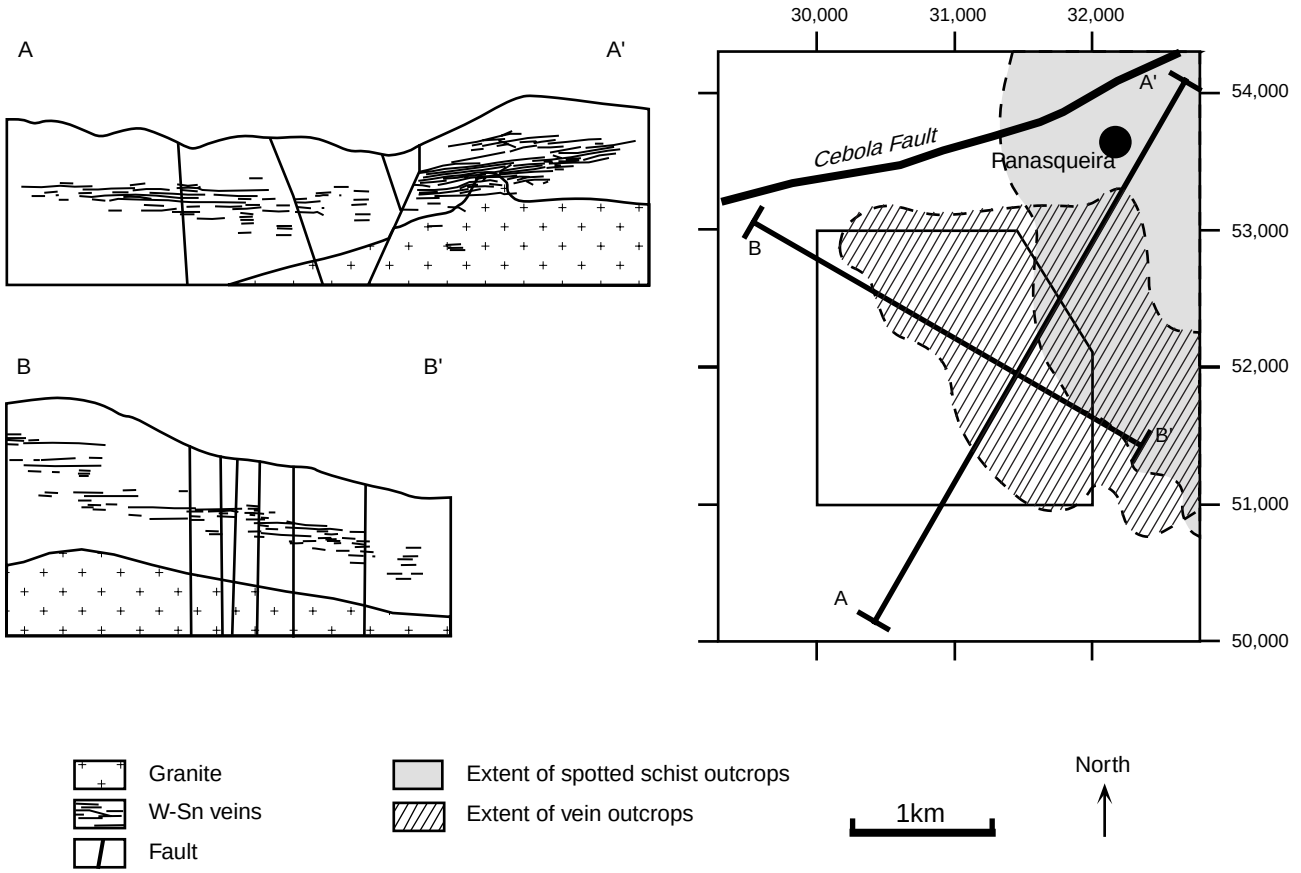

Fig. 3. Geological map of the Minas da Panasqueira locality with strike (A–A′) and dip (B–B′) sections illustrating the distribution of worked veins. The dip section has a vein-array angle (the plunge of the line connecting vein centres) of 12° SE, parallel to the surface of the underlying granite. The polygon inset into the geological map is used as a reference frame in later figures. Grid numbers are Portuguese National Grid.

greisenised, give an ^{40}Ar–^{39}Ar muscovite age of 292 ± 0.8 Ma (Snee et al., 1988), and are cut by the veins (Fig. 3). Individual veins consist predominantly of quartz (>90%); but wolframite (0.8%), cassiterite (0.04%) and chalcopyrite (1.1%) are present in amounts justifying commercial exploitation (Polya, 1989).

For the purposes of this work the paragenesis (Table 1) has been given a structural context (Fig. 4). Vein opening spanned the quartz–tourmaline (QT), main oxide–silicate (MOSS) and main sulphide (MSS) stages. Vein geometries indicate $\sigma_v = \sigma_3$ implying a horizontal compressional regime at this time (Kelly and Rye, 1979). The age and duration of QT mineralisation and its associated physiochemical conditions are poorly constrained. The MOSS and MSS mineralisation spanned a 3.4 Ma interval between 296 and 292 Ma (Snee et al., 1988), formed at fluid temperatures

Table 1
Simplified mineral paragenesis based on the work of d'Orey (1967), Kelly and Rye (1979), Polya (1989) and Foxford (1992)

Abbreviation	Paragenetic stage	Summary
QT (Oldest)	Quartz–Tourmaline	This stage is equivalent to the pre-vein stage of Polya (1989). Quartz and tourmaline with crack–seal textures were precipitated in newly formed fractures, i.e. at propagating vein tips.
MOSS	Main Oxide–Silicate	This stage encompasses the muscovite selvedge formation (MSF) stage of Polya (1989) and is characterised by the growth of muscovite, topaz, wolframite, quartz and arsenopyrite into rapidly opening veins.
MSS	Main Sulphide	Polymetallic sulphides, quartz and apatite were deposited during the climactic phase of vein opening
PAS	Pyrrhotite alteration	Pyrrhotite formed during the MSS was extensively leached resulting in the growth of pyrite, marcasite and siderite.
LCS (Youngest)	Late Carbonate	Dolomite, calcite and chlorite were precipitated in vugs within veins.

close to 300°C, with fluid salinities <10 wt.% NaCl equivalent and fluid pressures in the earliest precipitates close to 100 MPa (Kelly and Rye, 1979; Bussink, 1984). Polya (1989) calculated that to account for the mass of WO_3, 1000 km^3 of fluid must have passed through the vein system during the MOSS alone, the bulk of this fluid being of meteoric origin. Remnant vein porosity and permeability plays host to the youngest pyrrhotite alteration (PAS) and late carbonate (LCS) stage mineralisation, which was introduced into the veins via intersections with a swarm of similarly mineralised strike-slip faults, which dissect the damage zone and indicate $\sigma_v = \sigma_2$ at this time (Foxford, 1992). The PAS and LCS mineralisation formed at near hydrostatic fluid pressure (ca. 20 MPa), at lower temperatures (100–200°C) and lower salinities than the earlier QT, MOSS and MSS stages (Kelly and Rye, 1979; Bussink, 1984). Present day remnant vein porosities are large, perhaps 5%, and manifest as metre-scale vugs and smaller pores between vein-filling minerals.

2.2. The vein swarm

In profile view, W-bearing veins are sub-horizontal, co-planar and mutually overlap for much of their lengths (Fig. 3 sections A–A′ and B–B′). They constitute both a damage zone and an anomaly of positive volumetric strain of ellipsoidal form, >10 km^2 in lateral extent, extending through a depth interval of >0.75 km and containing veins with a volume of >0.1 km^3 (Kelly and Rye, 1979; Mello Mendes et al., 1987). The smaller vertical axis of the strain ellipsoid (ε_3) is parallel to both vein opening directions and (σ_3) at the time of veining. The major horizontal axis (ε_2) and the minor horizontal axis (ε_1) are in the plane of the veins. Vein geometries are consistent with brittle rock failure through injection of overpressured fluids (Kelly and Rye, 1979; Foxford et al., 1991a); vein walls are sharp and planar and the geometries of opposite walls match perfectly (e.g. Fig. 5a). During their propagation the veins evidently did not exploit any pre-existing structures, and although wall-rock

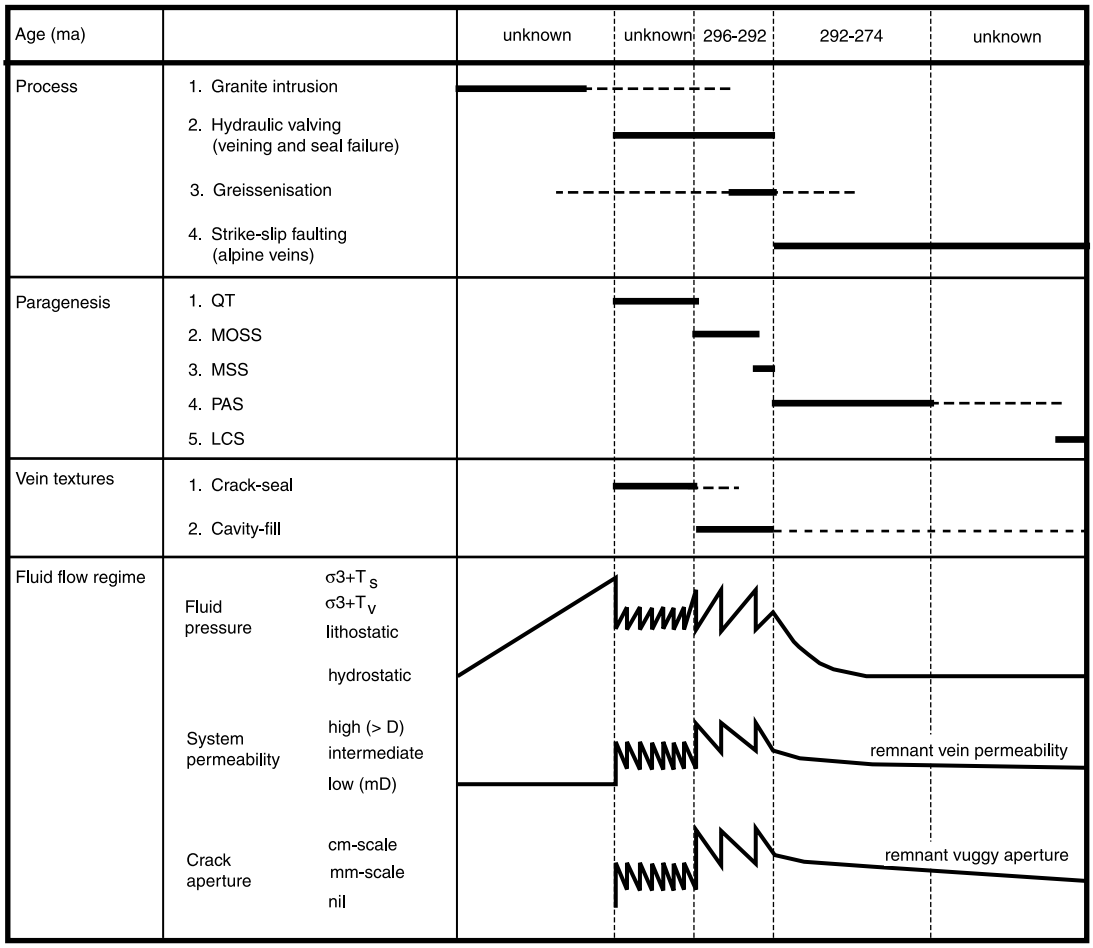

Fig. 4. Schematic sequences of events compiled from the data of Kelly and Rye (1979), Snee et al. (1988), Polya (1989) and Foxford (1992). For descriptions of paragenetic stages see Table 1.

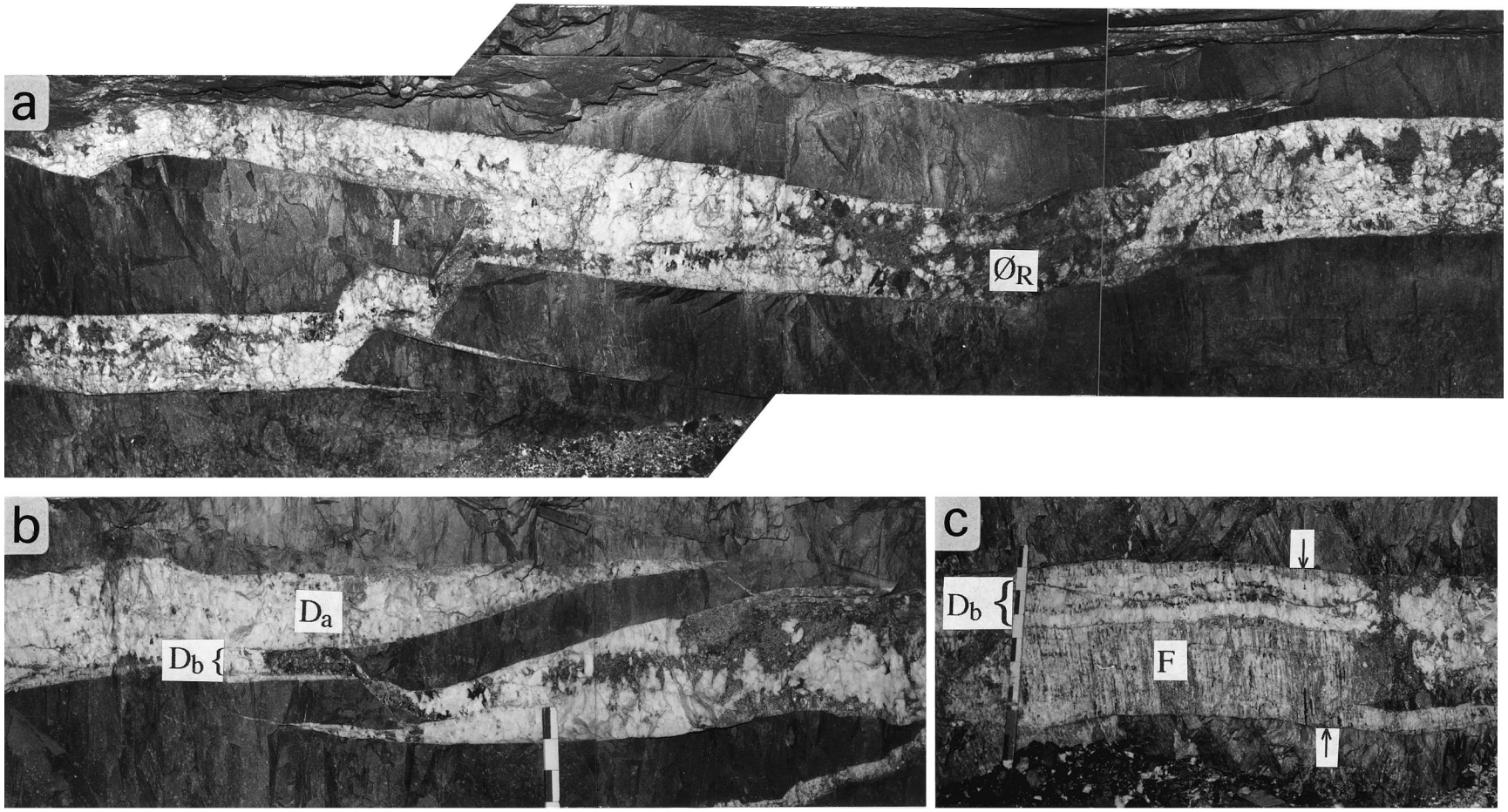

Fig. 5. (a) MOSS–MSS vein composed of linked right-échelon segments, the tabular bridge stubs being defined by splay veins. Note left-échelon splay vein in stope roof. Vein textures are massive but locally sheeted with MSS sulphides infilling remnant vuggy porosity ($Ø_R$) coincident with ruptured bridges (scale bar = 12 cm, aggregated vein thickness = 60 cm). (b) MOSS–MSS vein displaying localised coarsely sheeted texture. MOSS opening (D_a) accompanied bridge flexure whilst later syntaxial MSS opening (D_b) succeeded bridge rupture. Note the along-vein transition to massive non-sheeted textures (scale bar divisions = 10 cm). (c) MOSS–MSS vein with finely sheeted MOSS texture (F), indicative of a fluid flow baffle, cross-cut by a syntaxial MSS opening increment (D_b) displaying cavity filling texture. Arrows indicate apparent displacement of wall-rock bedding which parallels the mineral fibres. Note abrupt along-vein transition to massive cavity filling texture (scale bar divisions = 10 cm). (d and e) Photomicrograph pair (xp and ppl) of crack–seal QT vein. Inclusion bands are wall-rock slithers and/or metasomatic overgrowths of wall-rock muscovite, quartz, chlorite and tourmaline. Accretion increment thicknesses and quartz fibre width increases in the upper vein half and minor shear displacements are indicated by inclusion trails. Undulations in the upper vein wall formed through sequential calving of wall rock slithers from the upper margin during periods of antitaxial failure (vein thickness = 3 mm). (f) MOSS–MSS vein displaying non-sheeted (cavity filling) texture indicative of mineral growth into a large void: intra-crystal porosity between MOSS-stage wolframite (black) and quartz (white) is filled by MSS sulphides (vein thickness = 50 cm).

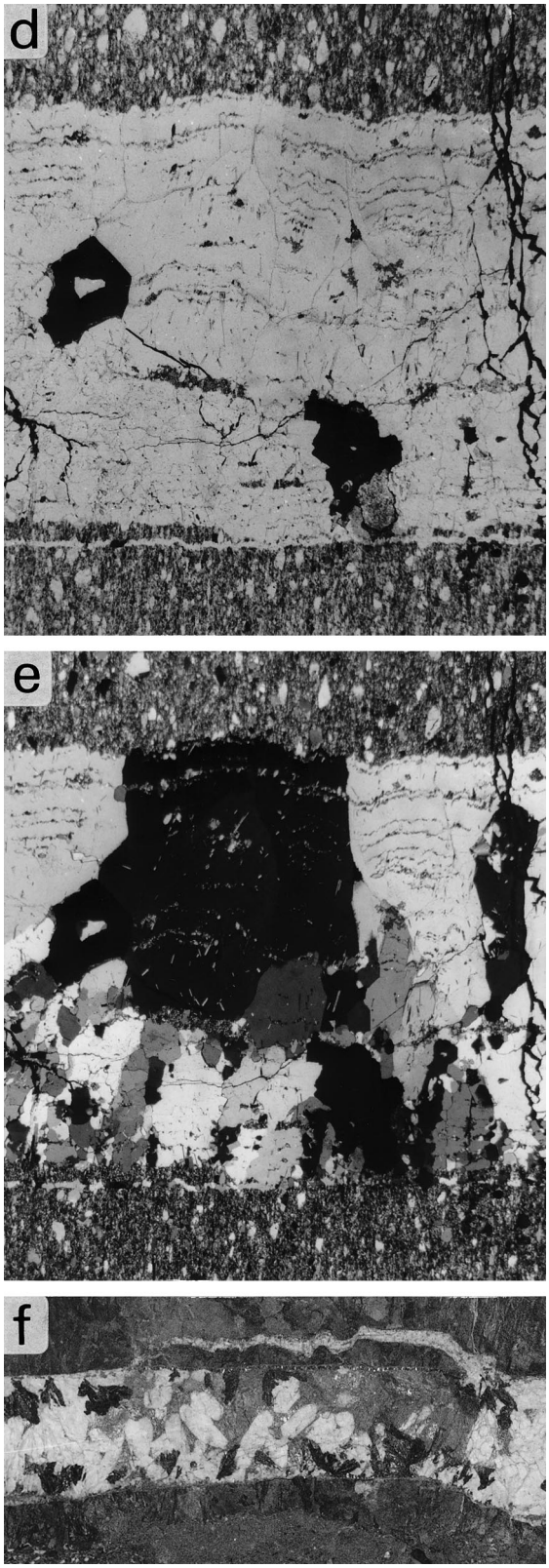

Fig. 5 (*continued*)

metasomatism produced extensive alteration halos of tourmalinised, muscovitised and chloritised schists around veins (Bussink, 1984), the shapes of vein-walls have not been modified in any significant way. Kelly and Rye (1979) noted that veins display helical geometries and numerous sub-horizontal splays that are important in linking vertically overlapping veins.

2.3. Vein descriptions

Two types of sub-horizontal veins are identified: older QT veins (quartz seams of Foxford et al., 1991a) containing QT mineralisation and younger MOSS–MSS veins containing QT–MOSS–MSS mineralisation. Spatial distributions of the mm-thick QT veins are poorly constrained but they form a dense swarm that outside of the Panasqueira vicinity is continuous with a similarly oriented joint swarm of regional extent (Kelly and Rye, 1979; Derre et al., 1986). Apparent vein lengths range up to a few metres and spacings are <1 m. Vein walls are generally planar and sub-horizontal with dips $<5^\circ$, although locally veins with dips $>30^\circ$ occur. Two sets of QT veins occur with conjugate angles between 10° and 30°. Together with rare 1–3 mm shear displacements across vein walls these features indicate vein growth under mixed-mode loading in the presence of a moderate differential stress ($\sigma_1-\sigma_3 > 4T$).

The MOSS–MSS veins define the damage zone and range in thickness from 1 cm to 1.3 m with vein lengths in the range from dm to >1 km. The veins are evidently compound (Fig. 5a and b), the subsidiary segments having apparent random stepping arrangements and sub-horizontal enveloping surfaces in profile view. Where three or more segments have the same stepping sense, twist angles are typically $<10^\circ$, although localised arrays with twist angles of up to 40° occur. Wall-rock bridges between segments facilitate vein thickness transfer and display no internal fabrics suggestive of significant shear strains. The QT mineralisation is preserved as remnant selvedges along one or both vein walls indicating that MOSS–MSS openings exploited earlier QT veins. Both QT and MOSS–MSS veins formed by one or more episodes of opening (e.g. Fig. 5b)

2.4. Vein textures and vein thickening

Detailed descriptions of vein textures were provided by Foxford et al. (1991a, b) and Foxford (1992). Textures of QT mineralisation are everywhere sheeted subparallel to vein walls at μm-scales (Fig. 5d and e). The MOSS–MSS vein textures are sheeted at μm–dm scales (Fig. 5b and c) only in lower portions of the damage zone; in its upper portions vein textures are non-sheeted (Fig. 5f). Both coarsely sheeted and finely sheeted textural types are identified; coarsely sheeted textures are restricted to MOSS–MSS mineralisation in vein centres whilst finely sheeted textures are restricted to QT and MOSS mineralisation adjacent to vein walls. The presence of multiple sheets of mineralisation, fibrous textures and inclusion trails suggests vein accretion through a type of crack–seal mechanism (cf. Grigorev, 1965; Ramsay, 1980; Cox and Etheridge, 1983; Cox, 1987, Henderson and Henderson, 1990).

Finely sheeted textures (Fig. 5c–e) are characterised by straight or gently sigmoidal quartz, wolframite and arsenopyrite fibres from 3 mm to 40 cm in length and up to 1 cm thick. Fibre parallelism with vein wall displacements (Fig. 5c) indicates fibre orientations approximate vein opening vectors. In profile view, quartz fibres are optically continuous under crossed nicols (Fig. 5d and e) and consist of quartz sheets, 10–300 μm thick, bounded by μm-thick bands composed either of wall-rock slithers, or included minerals such as white mica, tourmaline and optically non-continuous quartz grains. In individual quartz sheets, white mica, tourmaline, and the latter quartz grains form inclusion trails that track vein opening vectors indicating they grew into open space prior to inclusion into quartz sheets (cf. Cox, 1987). Quartz fibres contain several tens of accretion increments in QT mineralisation and many hundreds in MOSS mineralisation.

Coarsely sheeted textures (Fig. 5a–c) are characterised by mineral sheets with thicknesses in the range from 1 cm to >1 m. Veins with non-sheeted textures are filled by a single, continuous, mineral sheet. In individual mineral sheets deposited during a single accretion increment, older minerals such as wolframite are commonly found attached to vein walls and surrounded by younger deposits of quartz and sulphides (Fig. 5b and f). The crystals are euhedral and very large, up to 20 cm in diameter, and display competitive growth textures (drusy or cavity-filling textures) that are characteristic of coeval, competitive mineral growth into open space (cf. Grigorev, 1965; Berner, 1980; Dickson, 1983). Crystal fabrics are primary, as indicated by their twinned nature and contained ghost faces delineated by μm- to mm-scale fluid inclusions and crystals of tourmaline, white mica or sulphides (Foxford, 1992). Evidently, the fractures in which the sheet of minerals was deposited must have opened to their full thickness and maintained this until filling of the open space was complete.

Finely sheeted textures are predominantly formed via antitaxial vein-forming mechanisms whereby vein reactivation occurred along vein–wall-rock contacts (Ramsay and Huber, 1983, p. 245). In contrast, coarsely sheeted textures developed through both antitaxial and, more commonly, syntaxial vein forming mechanisms (Fig. 5a–c), the latter forming where vein reactivation occurred along vein centres (Ramsay and

Huber, 1983, p. 245). In both finely and coarsely sheeted textural types, antitaxial sheet boundaries are often delineated by vein-wall parallel schist slices, from μm to cm thick, torn from vein walls during episodes of vein opening and marking former positions of vein walls.

In lower reaches of the damage zone, the climactic sheet of accreted mineralisation is notably syntaxial, sulphide rich and contains the complete MSS. The increment is everywhere filled with cavity-filling texture and ranges in thickness from 1 cm to >40 cm (Fig. 5a and c). In higher reaches, this accretion increment is absent and MSS mineralisation is typically found as pods of euhedral crystals infilling remnant porosity between earlier mineral precipitates, the pods ranging in length from 1 cm to >5 m (Fig. 5a and f). These relationships illustrate that, in common with other episodes of vein accretion, MSS fluids reactivated all observable portions of the damage zone albeit with different expression at depth.

3. MOSS–MSS vein analysis

3.1. Geometrical coherence

Vein thickness profiles for entire subsidiary vein segments are bell-shaped due to tip-line confinement processes at zones of vein overlap (Fig. 6a and b). The aggregated profile confirms that the subsidiary segments evolved as a single structure whose opening-mode displacements were geometrically coherent and linked. Regular, systematic and predictable changes occur at all scales of observation. Thickness balancing explains the gentle gradient (0.002) of the aggregated thickness profile and the conclusion of Williams (1985) that vein thickness behaves statistically as a regionalised variable, being essentially constant for distances of up to 40 m along worked vein portions.

Profiles constructed using data for worked vein lobes (Fig. 7) are often less regular (e.g. red and black veins) than those for individual segments measured in stope faces; the saddles and cusps result from interaction with neighbouring vein lobes, kinematically a part of the worked vein but whose component of thickness is missing from the data set because the lobes were not mined. The aggregated profile (Fig. 7c) appears more regular and approaches the ideal bell shape illustrating that even at this scale vein thickness behaviour is geometrically coherent. Regions of steep vein thickness gradient (>0.05) are spatially associated with large-scale bridges, which transfer dilation between overlapping but separately worked veins. There is no evidence, such as an abrupt step in the aggregated thickness profile, to suggest that the saddles and cusps result through displacement transfer onto faults.

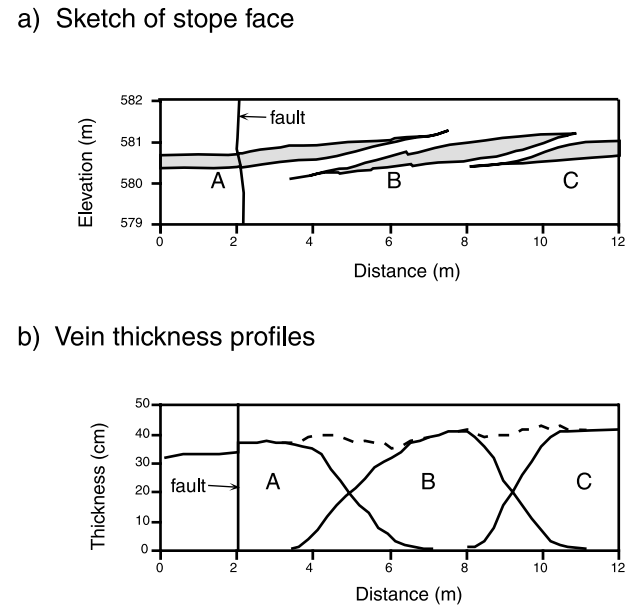

Fig. 6. (a) Section and (b) thickness profiles for vein segments in the stope face. Dashed line shows aggregated displacements for zones of segment overlap.

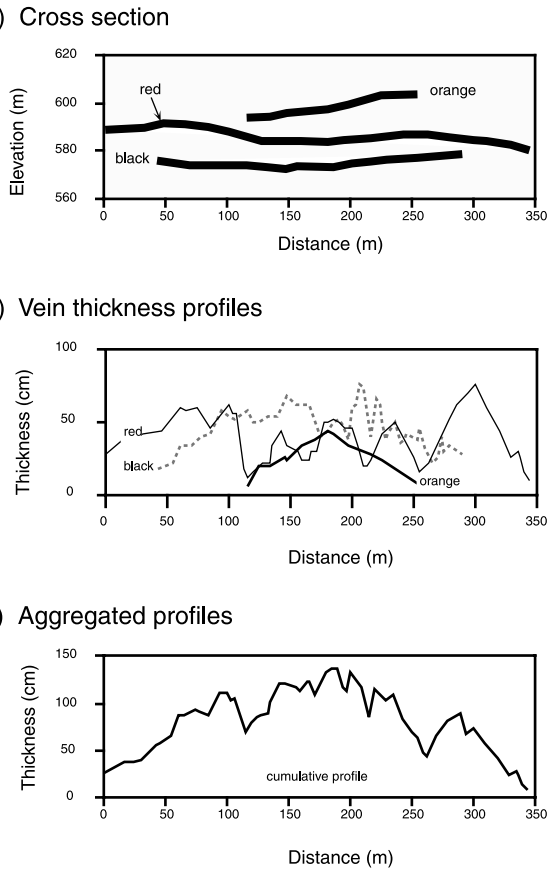

Fig. 7. (a) Section, (b) thickness and (c) aggregated thickness profiles for mutually overlapping worked veins.

3.2. Morphology and thickness distributions

In plan view, vein shapes are characteristically lobed and somewhat elliptical (Fig. 8). The structure contour map (Fig. 8a) illustrates the complex vein morphologies; each stope exploits a family of undulatory or gently dipping lobes that intersect at branch-points. Lobe enveloping surfaces have >10 m relief and distinct structural culminations and depressions despite being composed of numerous sub-horizontal components. This surface topography is inherited from the geometrical arrangement of QT vein arrays selected for MOSS–MSS opening. The branch points are characterised by helical vein geometries, as indicated by radial structure contour patterns, and in the figure provide important links between vein lobes with vertical separations exceeding 7 m and whose overlaps exceed 70 m long and 50 m wide. Despite extensive observations, we find no evidence for the existence of isolated vein lobes and we infer that all veins in the

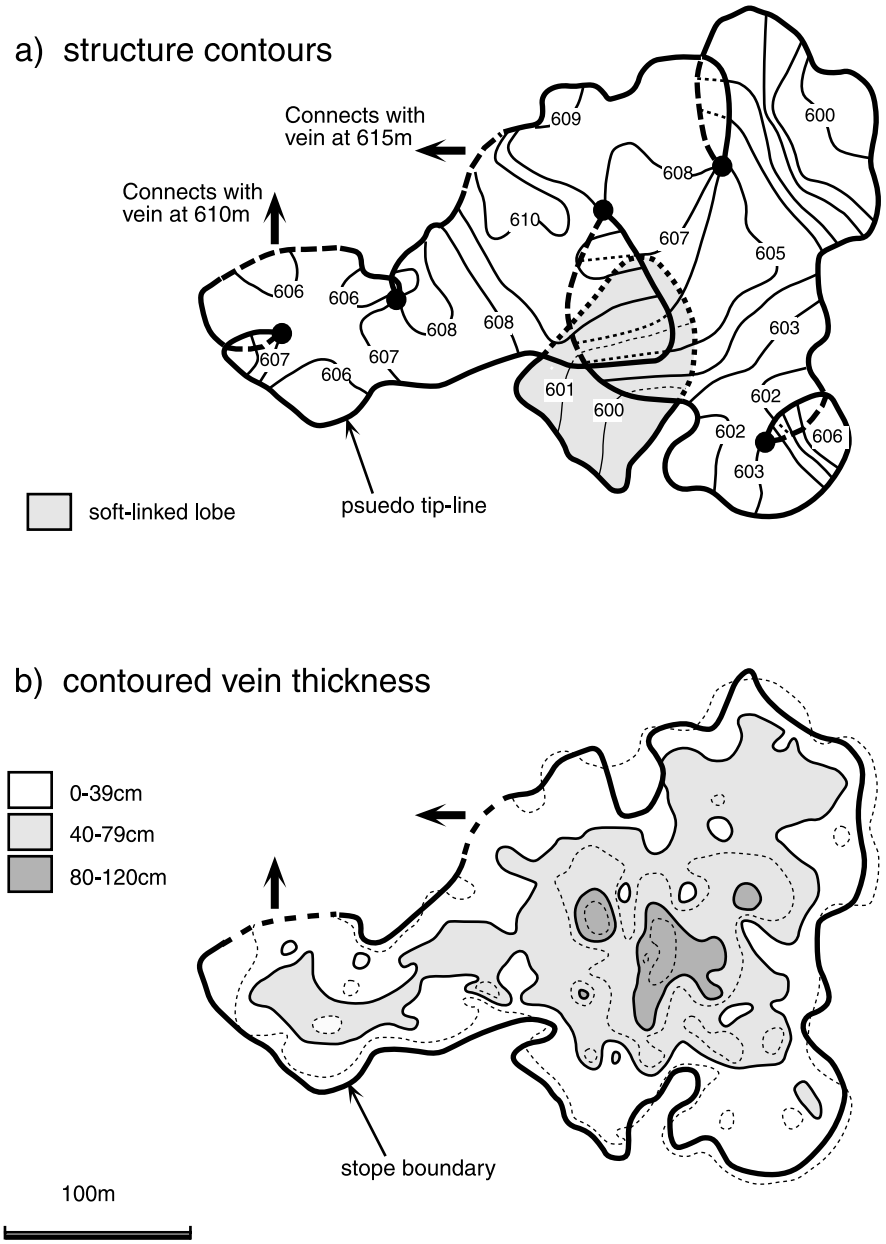

Fig. 8. Structure contour and vein thickness distributions (vein L2D25R2AW21. 600–610 m msl). Links with overlapping vein lobes are arrowed. (a) Structure contours drawn at 1-m intervals on top-enveloping surfaces of worked vein-lobes. Contours are dashed on overlapped surfaces. Lobe pseudo tip-lines are drawn at vein thickness 15 cm and are also dashed on overlapped surfaces. (b) Contoured vein thickness distribution derived by plotting thickness onto a horizontal projection of the top-vein surface. Thicknesses for worked portions of vein overlaps have been aggregated. The figure utilises several hundred measurements that are relatively regularly distributed along a grid of approximately 17 m spacing.

swarm are connected by tip-line bifurcation mechanisms into a single linked unit. Demonstration of this point is outside the scope of this paper.

The distribution of contoured vein thickness (Fig. 8b) is similar to that shown by Foxford et al. (1995, figure 6B) for an adjacent stope; vein thickness is distributed symmetrically, regularly and predictably, ranging from a maximum near the vein centre to ca. 10 cm at its edge, an artificial cut-off marking the minimum worked vein thickness. Contours of equal vein thickness are concentric and sub-parallel to the margin of the mine workings suggesting that the vein's tip-line loop is also sub-parallel to the margin of the mine workings. Steep contour gradients and localised depressions in vein thickness values are probably artefacts spatially coincident with unworked vein tips and subsidiary vein segments whose component of thickness is missing from the diagram.

3.3. Vertical extensional strain

At Panasqueira, because vein opening directions are sub-vertical, aggregated vein thickness (V_t) measured parallel to vein opening directions (parallel to ε_3) provides a bulk measure of vertical extensional strain (ΔL), here calculated as a percentage extensional strain $\Delta L = e \times 100$ where:

$$e = \frac{L_f - L_i}{L_i} = \frac{V_t}{L_i} \quad (3)$$

and where L_f is damage zone thickness, defined as measured from the base of the lowermost-vein to the top of the uppermost-vein, and L_i the pre-failure thickness of the damage zone given by $L_i = L_f - V_t$. In order to determine the nature of the strain anomaly, values of ΔL have been derived for the numerous sub-vertical drillcores that intersect the vein swarm (Figs. 9–11). The strain distributions are representative of MOSS–MSS failure when the majority of vein thickness was accreted.

The anomaly-scale distribution of ΔL (Fig. 9) closely resembles that shown for individual veins in Fig. 8(b). Centrally located ΔL maxima, which locally exceed 1%, are surrounded by elliptical but lobed contours of equal ΔL. Although the marginal areas of the ellipse are poorly defined, ΔL presumably decreases to zero at a sub-elliptical tip-line loop. We compare this distribution with those derived from numerous exploratory drillcores and truncated to include veins (1) >5 cm thickness (Fig. 10) and (2) >20 cm thickness (Fig. 11).

Fig. 10 utilises V_t data from short exploratory drill-

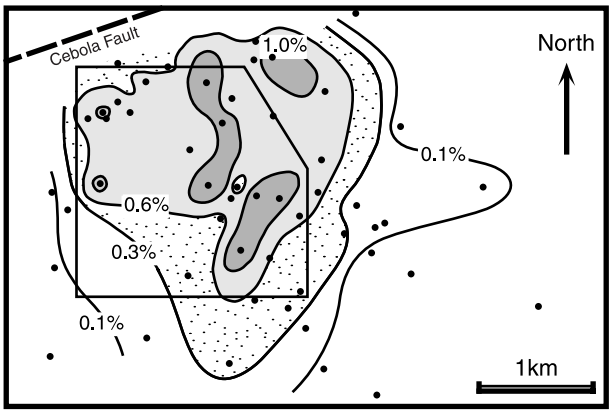

Fig. 9. Distribution of ΔL derived from veins >1 cm threshold thickness derived from 51 sub-vertical drillcores which completely transect the vein swarm. Values of ΔL have been projected onto a horizontal plan of the mine locality and contoured (data from Hebblethwaite and Antão, 1982).

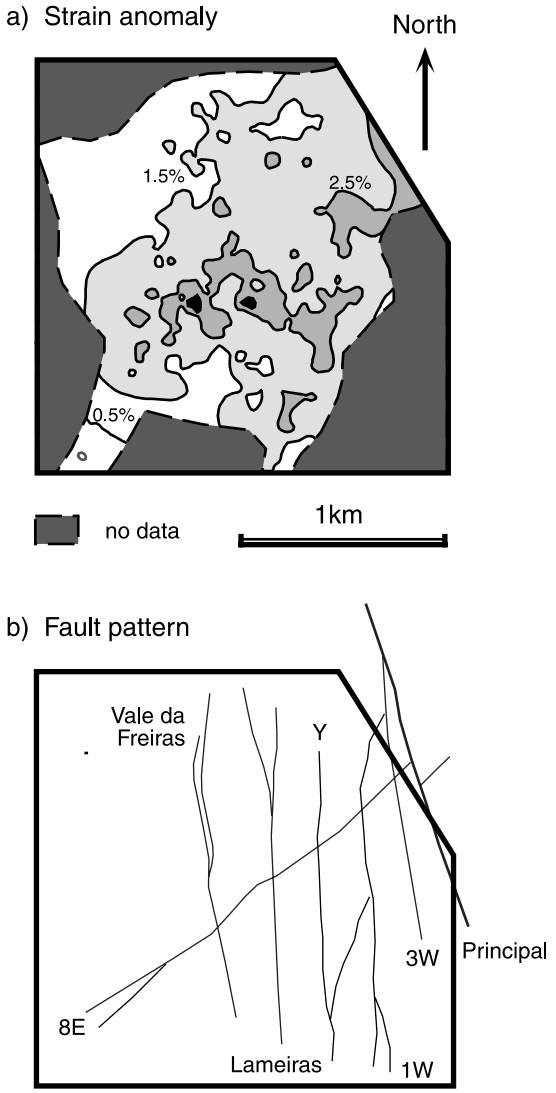

Fig. 10. Distribution of ΔL derived from veins >5 cm threshold thickness utilising 981 datapoints from sub-vertical exploratory boreholes. Values of ΔL are projected onto a horizontal plan of the strain anomaly and contoured (data from Hebblethwaite and Antão, 1982). (b) Principal strike-slip faults encountered in mine workings.

cores predominantly located in the high-strain core of the damage zone and each of which intersects a mine level. Data for each level have been gridded and the resulting surfaces aggregated and converted into ΔL values assuming $L_f = 180$ m, since, at this scale of investigation, the damage zone typically intersects no more than three mine levels. The resulting ΔL pattern is similar to that in Fig. 9 except that ΔL values locally exceed 3.5%, primarily because of the relatively small L_f value used in the calculation. Depressions in the contour pattern mark regions of strain deficiency, which may result either through incomplete drillcore sampling or through the presence of numerous veins < 5 cm thick. If threshold vein thickness could be lowered to include mm–cm-thick veins it is likely that the distribution of ΔL would appear much more regular. The gross vein thickness gradient, the maximum V_t (ca. 4 m) divided by the short axis of the ellipse (ca. 2 km), is 0.002, similar to that of individual veins.

The distribution of ΔL shown in Fig. 11 assumes all veins have a constant 20 cm thickness and $L_f = 180$ m. Although providing only a gross approximation of ΔL the figure provides constraints on the geometry of the high-strain zone.

Common features of Figs. 9–11 are that (1) the distribution of strain is broadly symmetrical and decreases regularly and predictable towards zero at the anomaly's edge, presumably defined by a zero strain tip-line loop, (2) the amplitude of lobed irregularities is small when compared to the extent of the anomaly, and (3) linear regions of steep strain gradient that may indicate a mechanistic relationship to high angle faults are absent. These factors are strong indicators that extensional failure was wholly consistent with brittle, elastic mechanisms.

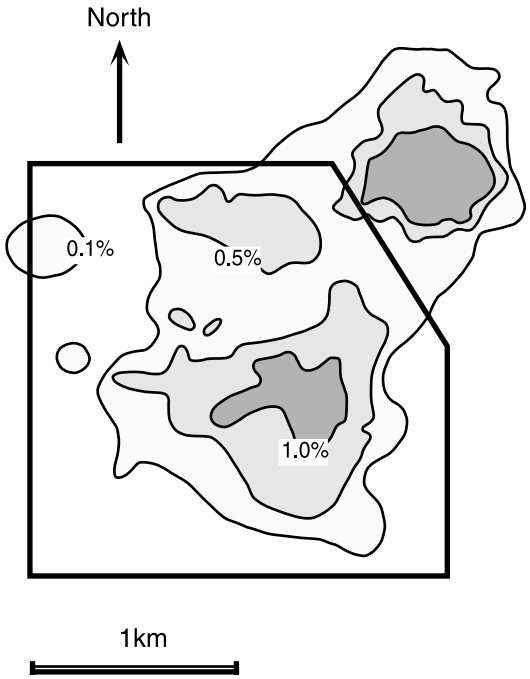

Fig. 11. Distribution of ΔL derived from veins > 20 cm threshold thickness. Values of ΔL have been projected onto a horizontal plan of the strain anomaly and contoured (data from Rodrigues, 1985).

3.4. Strain partitioning

The locations of 32 sub-vertical line transects used to define vein spatial distributions are shown in Fig. 12. The data for each are summarised in Table 2. The transects intersect the core of the damage zone and a significant portion of its surrounding marginal areas. Ideally, each transect would be a single drillcore that completely intersects the damage zone but, since these are relatively limited, several pseudo-transects were compiled from short but closely spaced (< 10 m) and overlapping, drillcores. Although transect lengths are in the range from 110 m to > 500 m only between 14 and 34 veins > 5 cm threshold thickness are intersected in any single transect, and these are concentrated in the core zone. Despite these shortcomings, each transect has been analysed separately to avoid degrading the data and masking damage zone-scale variations in vein distributions and geometry.

Typical transects are summarised in Fig. 13 and suggest that the damage zone has a vertical thickness in the range from 160 to 300 m (Fig. 13a). The gradients of staircase plots (Fig. 13b) reveal the distribution of strain along each transect (cf. Gillespie et al., 1999) and provide a simple measure of the distribution of deformation in the extension direction. The plots are characteristically sigmoidal indicating that the distri-

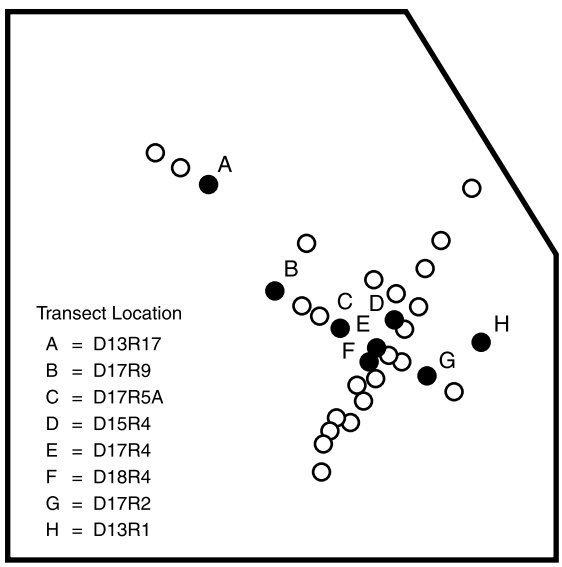

Fig. 12. Map of the inset polygon (Fig. 3) showing the locations of the 32 sub-vertical line transects used to constrain vein spacing and thickness distributions. Solid circles indicate transects referred to in text.

bution of strain is inhomogeneous; relatively few thick veins in the core zone account for the bulk of the measured extension. Similar plots from partial transects through fault-related damage zones consisting of non-stratabound quartz and calcite veins have been reported by (Gillespie et al., 1999). However, at Panasqueira, the plots define bi-modal deformation at a scale above that of the vein spacing; a homogeneously deformed high-strain core zone is enveloped by inhomogeneously deformed low strain marginal zones. The well-constrained core zone is ca. 110–150 m thick, contains most of the worked veins and has cumulative vein thickness gradients of 0.03 (Fig. 13c). The enveloping marginal zones are ca. 100–200 m wide, contain thin veins, have cumulative vein thickness gradients of 0.007 (Fig. 13d) and are poorly constrained.

Within the vein cluster, vein thickness and spacing populations (e.g. Fig. 14a and b) for the majority of the 32 transects are anticlustered and non-power law (Table 2). Coefficients of variance (C_v), the ratio of the standard deviation to the mean, have been used to characterise vein spatial distributions for each transect following the method described for $C_{v\ (\text{vein spacing})}$ by Gillespie et al. (1999) who demonstrate that for $C_v > 1$ veins are clustered, i.e. power-law; for $C_v = 1$ vein spacings are random; for $C_v < 1$ the spacings are anticlustered or periodic, whilst for $C_v = 0$ the veins are equally spaced.

At Panasqueira, the average $C_{v\ (\text{thickness})}$ and $C_{v\ (\text{spacing})}$ are 0.69 and 0.85, respectively, indicating anticlustered, periodic, spatial distributions. The range of $C_{v\ (\text{thickness})}$ is from 0.4 to 1.27; only a single transect containing one very thick vein has a power-law distribution ($C_{v\ (\text{thickness})} > 1$). The range of $C_{v\ (\text{spacing})}$ is from 0.38 to 1.83 and contains six transects with power-law spacings ($C_{v\ (\text{spacing})} > 1$), the remaining 26 transects display non-power-law behaviour. No statistically significant differences in $C_{v\ (\text{spacing})}$ or $C_{v\ (\text{thickness})}$ are apparent between those transects restricted to the core zone and those intersecting both core and marginal zones. Similar thickness and spacing populations have been reported from sets of dominantly opening-

Table 2
Summary data for the 32 line transects used to constrain vein spatial distributions (for transect locations see Fig. 12). C_v refers to coefficient of variance of the bracketed parameter, ΔL gradient refers to rate of change of vertical strain in the designated zone

Transect location	Length (m)	Vein intersections	C_v (vein spacing)	C_v (vein width)	ΔL gradient (core-zone)	ΔL gradient (upper marginal-zone)	ΔL gradient (lower marginal zone)
D3R4	180	14	0.65	0.40	0.013		
D9R4	150	18	0.77	0.62	0.018		
D11R4	190	21	0.77	0.63	0.015		
D15R4	140	24	1.24	0.63	0.038	0.0044	
D17R4	200	28	1.2	0.82	0.034		0.0066
D18R4	320	26	1.83	0.84	0.03		0.0023
D20R4	115	18	0.79	0.82	0.028		
D23R4(i)	120	14	0.74	0.44	0.034		0.0064
D23R4(ii)	100	15	0.38	0.90	0.026		
D24R4	120	20	1.06	0.66	0.029		0.006
D25R4	130	19	0.76	0.64	0.041	0.0069	0.008
D13R3A	90	18	0.73	0.69	0.03		
D15R3A	110	14	0.62	0.73	0.028		
D17R3A	120	17	1.03	0.64	0.026		
D19R3A	130	18	0.92	0.60	0.027		
D21R3A	140	18	0.92	0.88	0.036		0.005
D23R3A	80	14	0.64	1.27	0.035		
D27R3A	45	16	0.75	0.70	0.039		
D17R1	130	16	0.84	0.94	0.048	0.008	
D17R2	150	20	0.74	0.77	0.02		
D17R3	150	24	0.94	0.73	0.028		
D17R5A	170	29	0.79	0.58	0.041	0.008	0.007
D17R5BA	150	24	0.75	0.91	0.049	0.01	0.01
D17R6	110	23	0.92	0.72	0.06		0.0056
D17R9	115	29	0.67	0.73	0.043		
D13R1	260	21	0.98	0.80	0.031	0.011	0.006
D13R4A	220	25	0.88	0.69	0.033	0.0025	0.008
D13R5A	190	21	0.81	0.48	0.027	0.006	
D13R9	150	19	0.87	0.59	0.018		
D13R17	270	34	0.68	0.57	0.033	0.01	0.01
D13R19	150	21	0.87	0.50	0.013		
D13R21	150	16	1.02	0.48	0.009		

mode, stratabound veins from SW England (Gillespie et al., 1999).

There appears to be no simple relationship between vein spatial distributions (Figs. 13 and 14) and patterns of vertical strain (Figs. 9–11). The strain maxima of Figs. 9–11 are only broadly coincident and suggest that veins >20 cm thickness are deficient in regions of high strain in uppermost levels of the damage zone, e.g. in the NW corner of the figures. Vein transects also indicate that as threshold vein thickness increases so vein spacing increases (Fig. 13a). These spatial characteristics are supported by a statistical analyses

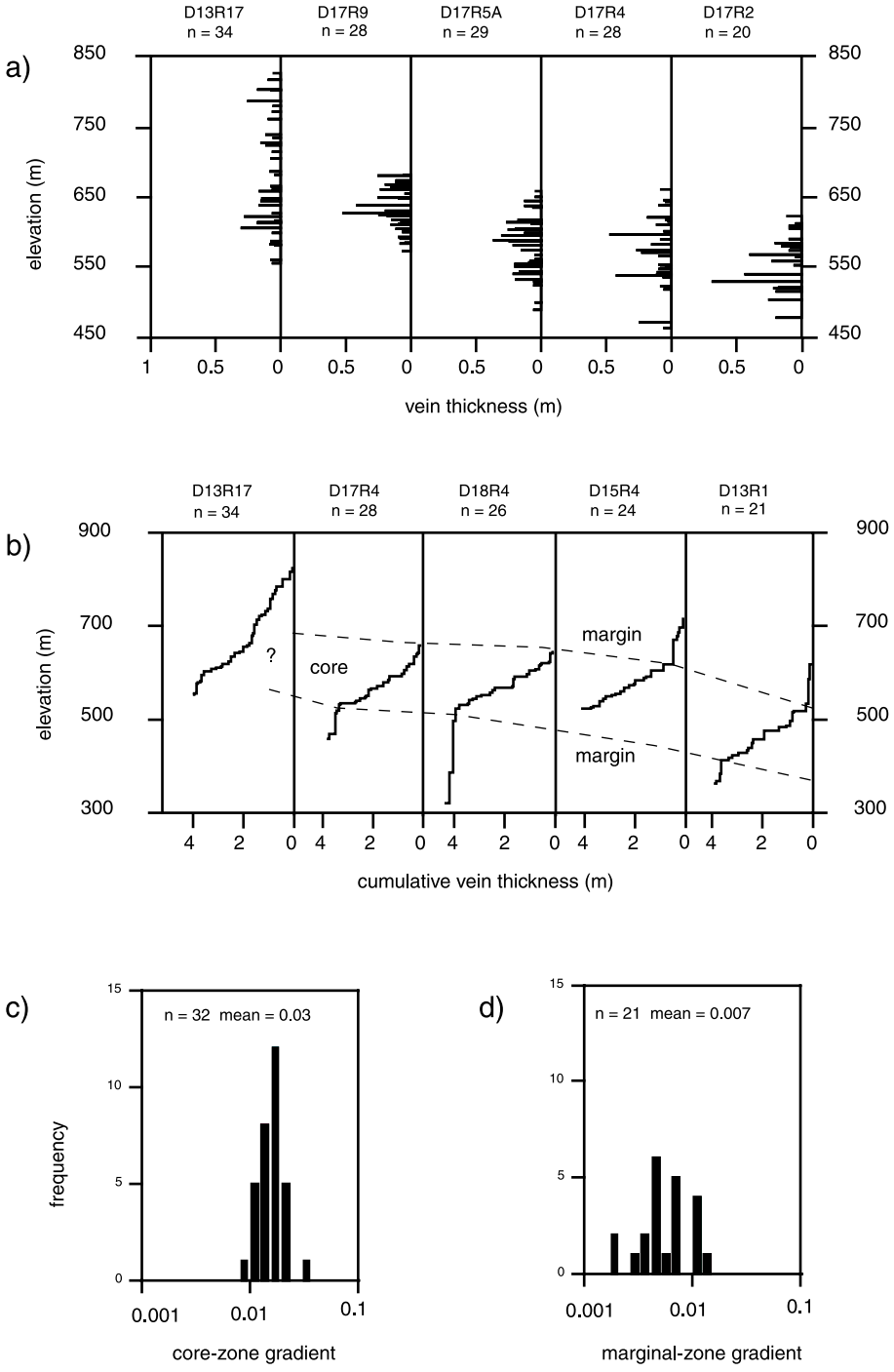

Fig. 13. Damage zone-scale variations in vein spatial distributions derived from line transects. (a, b) Transects arranged along sections similar to B–B′ in Fig. 3 showing (a) vein spacings and thicknesses, each bar represents the thickness of a vein and the elevation of its midpoint, and (b) staircase plots, i.e. plots of cumulative vein thickness (top-down) against vein elevations, showing the distribution of extensional strain. (c, d) Simple histograms showing frequency data for core- and marginal zone gradients of cumulative vein thickness (for transect locations see Fig. 12).

of mine records by Williams (1985, p. 153 and178) who found, for veins >1 cm threshold thickness, that (1) mean vein thickness increases with depth in the damage zone from 9.0 cm in its uppermost reaches to a maximum of 14.8 cm in lower levels, and that (2) despite a mean vein spacing of 7 m, vein density concordantly decreases with depth from 0.28 veins m^{-1} in the uppermost reaches to 0.08 veins m^{-1} at lower levels. A similar trend to increasing vein thickness with depth has been reported from W-bearing quartz veins at Chojlla, Bolivia (Harwood, 1985).

4. Discussion

4.1. Conceptual mechanical model

The absence of significant shear strain, wall-rock metasomatism and pressure dissolution enables the geometric, displacement and textural data to be amalgamated within a simple elastic fracture mechanics framework for damage zone development.

4.1.1. QT veining

Initial failure accompanied formation of a conjugate swarm of crack–seal QT veins. The veins grew as mixed-mode (?dominantly extensional) fractures under conditions where $P_f = \sigma_3 + T$. Vein geometries and opening vectors imply a compressive regime with $\sigma_3 = \sigma_v$, $\sigma_1 - \sigma_3 \geq 4T$ and $\lambda_v \rightarrow 1$. The dominantly antitaxial vein thickening mechanisms (Fig. 5d and e) indicate that once veins had nucleated, their vein–wall-rock contacts became the primary planes of weakness accommodating repeated extensional failure. Formation of QT veins might represent either (1) a separate early phase of fluid overpressuring, or (2) the distal propagating tips of MOSS–MSS macrocracks (cf. Nicholson, 1991; Foxford et al., 1991a).

4.1.2. Competitive MOSS–MSS veining

The MOSS and MSS periods of vein growth represent hydraulic (mode-I) reopenings of a selected QT veins at overpressures with $\lambda_v \geq 1$ and at differential stresses $<4T$. The kinematic and geometric coherence of MOSS–MSS vein accretion results from competitive vein forming mechanisms that provide (1) a preferential growth mechanism that localised deformation onto a few evenly spaced veins, and (2) a mechanism for inhibiting vein nucleation. Competitive vein forming mechanisms explain why vein spatial distributions show deviations from power-law behaviour similar to those reported from other mineralised vein systems in non-layered rocks (e.g. Sanderson et al., 1994; Roberts et al., 1999; Gillespie et al., 1999).

As the damage zone evolved it became saturated with veins, i.e. neighbouring vein lobes overlapped

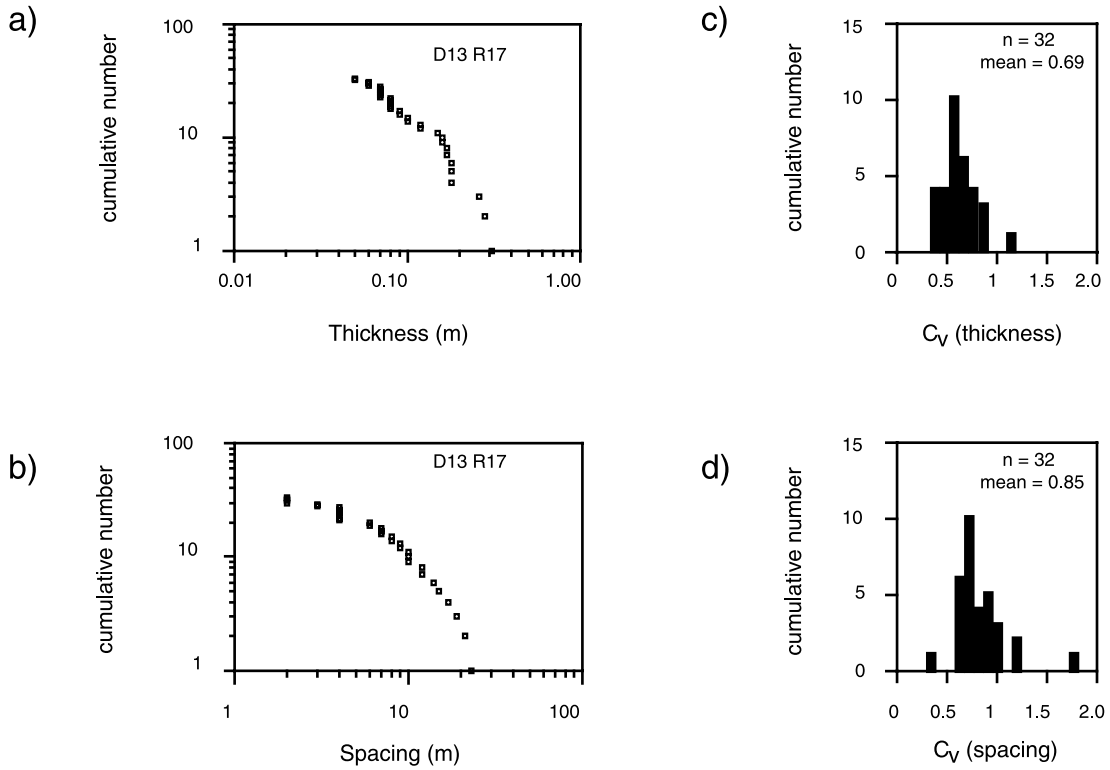

Fig. 14. (a) Thickness and (b) spacing populations for transect D13R17 (for location see Fig. 12). Coefficients of variance (C_v) are 0.57 and 0.68, respectively. Also shown are simple histogram populations of (c) $C_{v\ (thickness)}$ and (d) $C_{v\ (spacing)}$ for all 32 analysed transects (see Table 2).

leading to tip-line confinement and kinematic interdependence (e.g. Olson and Pollard, 1991). Kinematic interdependence provides a mechanical switch that lowers the Young's Modulus (cf. Main et al., 1990) and links adjacent vein lobes by promoting bridge flexure and eventually rupture (Nicholson and Pollard, 1985; Foxford et al., 1991a). This switch abruptly increases effective vein lengths and, because fracture thickness scales with fracture length (Pollard and Segal, 1987; Vermilye and Scholz, 1995), promotes accelerated rates of vein opening when compared to those rates possible for shorter, isolated, veins.

Segal and Pollard (1983), Olson and Pollard (1989) and Olson (1993) have shown that as veins grow larger, they (1) place smaller neighbours into their stress shadows, i.e. regions surrounding them, but distal to their tips, in which levels of effective tensile stress are reduced inhibiting either nucleation or growth of smaller, overlapped, veins, and (2) progressively interact with more distant neighbours. At Panasqueira, the regular spacing and mutual overlaps of worked veins (Fig. 3) indicate that the size of stress shadows did not scale linearly with vein length but was restricted in some way, perhaps by reduction of the Young's Modulus (cf. Gross et al., 1995).

The regular spacings and mutual overlaps also suggest that strain rates during veining were relatively high (Wu and Pollard, 1993), as might be expected when $\lambda_v \geq 1$. Additional support for failure at high strain rates is provided by the presence of a vein swarm since the growth of a single vein was evidently insufficient to relieve the tensile stresses developed within the damage zone (cf. Grady and Kipp, 1987). However, a scale effect exists since when viewed at the damage zone-scale the displacement geometry of the vein swarm resembles that of a single extensional structure.

4.2. Fluid sources and fluid flux

Although the ultimate causes of fluid migration and hydrothermal circulation are outside the scope of this paper, oxygen isotopic signatures of the QT mineralisation are consistent with episodic precipitation from high pressure magmatic fluid (Polya et al., 2000). This suggests initial schist failure was accomplished through the $P\Delta V$ of a magmatic fluid that segregated at near lithostatic pressures through phase changes and exsolution of volatiles accompanying crystallisation of near surface portions of the Panasqueira intrusion (cf. Burnham, 1985; Halls, 1987). The isotopic signature of MOSS–MSS mineralisation suggests that selected QT veins were later exploited by hydrothermal fluids of meteoric origin (Kelly and Rye, 1979; Polya, 1988, 1989). To accommodate a MOSS fluid flux of ca. 1000 km^3 (Polya, 1989), the damage zone must have been an open system, i.e. hot, buoyant fluids injected into its lowermost reaches were extruded via its uppermost reaches, the fluid presumably becoming part of the background hydrothermal flux that recharged the system. The nature of these recharge processes are beyond the scope of this paper.

4.3. Distribution of opening mode displacements and vein aperture

The Panasqueira vein textural data show that considerable discretion is required when using accretion increment distribution to assess either vein aperture (e.g. Vermilye and Scholz, 1995) or spatial distributions of opening-mode displacements (e.g. Davison, 1995). Vein textures relate to vein aperture through an interplay between rates of cavity opening and rates of mineral filling (Grigorev, 1965; Cox and Etheridge, 1983; Henderson and Henderson, 1990; Fisher and Byrne, 1990; Urai et al., 1991; Foxford et al., 1991a, b). For an extensional vein accommodating brittle/elastic failure and subject to constant rate of mineral-filling, finely sheeted textures will predominate where rates of opening are outpaced by rates of mineral filling (e.g. at vein tips), and coarsely or non-sheeted texture where rates of opening outpace those of mineral filling (e.g. in vein centres). In any single location these textural changes also reflect successive stages of vein evolution with time (Foxford et al., 1991a). In locations where vein textures are sheeted, fracture apertures were transient; their maximum thickness approximated by mineral accretion increment thicknesses. Where vein textures are non-sheeted, fracture apertures were large and persistent; their exact thickness depending upon the extent of mineral selvedges coating fracture walls.

At Panasqueira, if rates of mineral growth are held constant, vein aperture increased significantly over time: finely sheeted QT and MOSS textures at vein walls indicate initial apertures of 10–200 μm, whilst coarsely sheeted MOSS–MSS textures in vein centres indicate climactic apertures of up to 1.3 m. Such temporal variability is wholly consistent with competitive vein formation whereby initial unconfined vein growth is superseded by kinematic interdependence and rapid opening of a few through-going veins. Similar bimodal vein opening histories have been reported elsewhere (Nicholson, 1991; Clark et al., 1995).

Vein aperture was also spatially variable at the damage zone scale. Firstly, non-sheeted MOSS mineralisation in the zone's upper reaches indicates substantial apertures, whilst sheeted MOSS textures in the lower reaches indicates consistently smaller apertures. Secondly, in the deeper reaches, the MSS provides evidence for substantial climactic apertures locally exceeding 40 cm, whilst in the upper levels MSS apertures

consisted of vuggy porosity in partially cemented veins. Thirdly, abrupt transitions along veins from finely to coarsely sheeted textures (Fig. 5b and c) are inferred to indicate similarly abrupt variations in aperture. However, abrupt textural transitions might be explained by any of three options: (1) abrupt spatial variations in opening-mode displacements, (2) extensive dissolution of finely sheeted texture producing pockets of dissolution porosity into which non-sheeted texture grew, or (3) coeval growth of sheeted and non-sheeted textures through spatial variations in rates of mineral deposition (cf. Foxford et al., 1991a). The textural changes cannot be explained by option (1) because this would be inconsistent with the coherent nature of brittle/elastic deformation. We rule out option (2) since, despite extensive observations, we find no evidence for significant dissolution of either finely, coarsely or non-sheeted textures. Textural evidence for infilled vugs is common in coarsely and non-sheeted textures (Fig. 5a, b and f), but lacking in finely sheeted textures. Where vugs occur, their walls contain the full QT–MOSS–MSS paragenetic sequence and display euhedral crystals suggesting vugs did not form as dissolution features. Evidence for limited dissolution of vug minerals is found only when PAS and LCS mineralisation is present. We therefore conclude that the textural variability is best explained by option (3).

Rates of mineral growth are known to be inherently variable depending upon nutrient supply, number of crystal nuclei or seed fragments, crystallographic orientations and rates of fluid flow (Grigorev, 1965; Berner, 1980; Dickson, 1983; Fisher and Byrne, 1990; Henderson and Henderson, 1990). At Panasqueira, we infer that fractures were most rapidly filled where minerals were most favourably positioned and orientated for growth resulting in vein portions with transient, small aperture. In intervening areas fracture filling was slower and aperture larger and longer lasting because either rates of mineral nucleation were restricted (e.g. seed fragments or suitable substrates were sparse) or levels of fluid supersaturation reduced (e.g. through mineral growth in downstream regions). Abrupt spatial variations in fracture aperture resulting from spatial variations in rates of mineral deposition have been reported from gold-bearing veins of the Meguma Group, Nova Scotia (Henderson and Henderson, 1990).

4.4. Hydraulic valving

We envisage extensional failure as a dynamic process involving fracture propagation within supralithostatic pressured portions of a Beira Schist seal lying beneath the hydrostatically pressured regime (cf. Cox et al., 1991). The ΔL patterns do not resemble the underlying pluton geometry and suggest hydraulic failure was not related to contraction of the underlying pluton during cooling (cf. Sillitoe, 1985; Derre et al., 1986). Extensive greisenisation provides evidence that the granite was sufficiently permeable locally to provide a migration pathway beneath the seal.

Hydraulic valving initiated when fluid migration through the granite was sufficiently impeded by the seal to promote overpressures with $\lambda_v > 1$ and failure at the schist–granite contact when $P_f = \sigma_3 + T_s$ (Fig. 15). Vein distributions imply hydraulic failure was largely inhibited within the granite because $T_s < T_g$, where T_g is the tensile strength of the granite. Failure at the base of the seal introduced dynamic, fracture-hosted permeability reducing effective seal thickness. The zone of hydro-fracturing propagated upwards as long as fluid pressures with $P_f = \sigma_3 + T_s$ were maintained at propagating fracture tips. The MOSS–MSS vein swarm is restricted within a limited vertical interval (750 m) controlled by the magnitude of T_s, the near hydrostatic pressure gradient (albeit at near lithostatic levels) in the fracture-permeable damage zone and rates of fluid egress through the seal (Fig. 15). Continued upwards propagation of MOSS–MSS veins was inhibited because pore pressure at the base of the seal was no longer sufficient to support fracture apertures (i.e. $\lambda_v < 1$) promoting fracture closure and fluid pressure build-up beneath the seal. Maximum fluid pressure was therefore buffered to $P_f = \sigma_3 + T_v$, where T_v is the tensile strength of antitaxial or syntaxial vein failure planes and where $T_v \ll T_s$ (Sibson, 1981), the exact value of T_v depending on the degree of damage zone cementation. Fluctuations in pore pressure associated with fracture opening were probably limited to values $\simeq T_v$, i.e. a few MPa.

The model explains the damage zone's key vein textural features. The MSS mineralisation provides clear evidence that batches of fluid were able to permeate the entire damage zone and that dynamic pressure fluctuations, required for fracture reopening and sheeted texture formation, were only promoted at depth in the zone. In the zone's upper reaches, overpressures with $\lambda_v > 1$ prevailed, essentially inflating fractures in a single event and leading to formation of non-sheeted textures. Fracture apertures here were persistent and supported by pore pressure, probably aided by compressive stress and mineral cements. Despite extensive investigations we have found no textural evidence for abrupt aperture collapse such as might indicate a complete failure of the seal and decompression of the system to the hydrostatic regime.

Sheeted textures are indicative of hydrothermal self sealing of fracture permeability, a process that controlled the development of high fluid pressure domains within and below the lower portions of the damage zone (cf. Cox et al., 1991). Production of high fluid pressure domains was important at Panasqueira

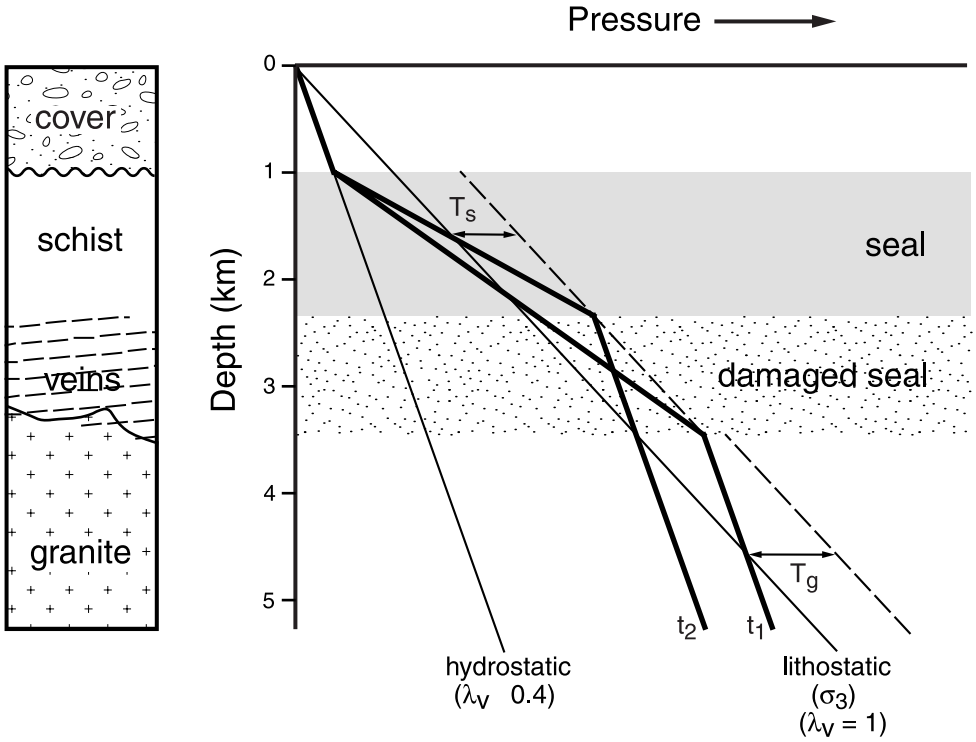

Fig. 15. Schematic diagram of depth-dependent P_f at two key times during the development of a damage zone consisting of co-planar, sub-horizontal veins: time t_1 is when hydraulic failure is initiated at the base of the seal when $P_f = \sigma_3 + T_s$; t_2 is the later time at which hydraulic failure has extended to its uppermost limit defining the vertical extent of the zone. T_s and T_g refer to the tensile strengths of seal and granite, respectively. A relative lack of veins in the granite suggests $T_s < T_g$. Beneath the seal, P_f is supralithostatic with near hydrostatic pressure gradients (cf. Cox et al., 1991) at time t_1, hydrostatic pressure gradient are restricted to granite but by time t_2 the increase in permeability in basal portions of the seal enables hydrostatic gradients to extend to top damage zone levels. Cover rock thickness is unknown—this part of the section is included only to illustrate near surface P_f was likely ultimately to have decreased to near hydrostatic values.

because it lead to repeated vein reactivation (when $P_f = \sigma_3 + T_v$), promoting accelerated rates of vein accretion, in those portions of the damage zone that accommodated the greatest fluid flux, i.e. at depth in the zone where preferential cementation was promoted for example by fluid disequilibrium with schist wall rocks (de Caritat, 1990). Consequently, veins prone to self sealing accreted vein thickness at accelerated rates when compared to those rates possible for veins in the zone's upper reaches. Preferential self sealing at depth may explain the observed trends to increased mean vein thickness, and decreased vein density, with depth in the zone (cf. Williams, 1985).

Although sheeted textures bear testimony to vein formation by locally episodic mechanisms, e.g. the climactic and mineralogically distinct MSS, textural characteristics alone cannot differentiate at the damage zone-scale between steady-state, systematically changing, or episodic and pulsatory extensional failure mechanisms. However, the textural evidence is consistent with both Snee et al.'s (1988) notion that MOSS–MSS mineralisation occurred as short lived pulses within a 3.4 Ma overall timespan, and current estimates of the durations of ore-forming pulses of 10^4–10^5 y (Cathles et al., 1997).

5. Conclusions

1. The Panasqueira vein swarm formed through extensional failure driven by hydraulic-valving at moderate differential stresses ($\leq 4T$) in a compressive crustal regime. The veins grew in the supralithostatic pore pressured region beneath a low permeability seal. The veins constitute a fracture-permeable damage zone characterised by positive volumetric strain.
2. Contoured patterns of vertical extensional strain define an elliptical anomaly with a centrally located maxima that diminishes regularly and systematically towards zero at a tip-line loop. The regular distribution and absence of linear zones of steep gradient suggest that failure did not exploit existing structural weaknesses such as faults.
3. In profile view, the distribution of linear strain is inhomogeneous and comprises a homogeneous high-strain core zone, with strain gradient $\approx$ 0.02, mantled by low strain marginal zones, with strain gradient $\approx$ 0.007.
4. Competitive vein forming mechanisms provide (i) a preferential growth mechanism that localised defor-

mation onto a few evenly spaced veins, and (ii) a mechanism for inhibiting vein nucleation. These mechanisms are required to account for deviations from power law vein thickness behaviour (e.g. Sanderson et al., 1994) and promote bi-modal vein opening histories whereby initial crack–seal growth is superseded by rapid vein opening.

5. Vein spatial distributions are non-power-law with the thickest veins evenly spaced and concentrated in a high-strain core zone.
6. Worked veins (i.e. vein >20 cm thickness) are collections of co-planar vein lobes that intersect at branch-points, the lobes forming during propagation by combinations of tip-line bifurcation and tip-line confinement processes.
7. Opening-mode vein displacements show kinematic and geometric coherence at all scales of investigation indicating that gross damage zone behaviour was that of a single extensional vein.
8. Contoured vein thicknesses are symmetrically distributed; thickness maxima are centrally located whilst thickness decreases regularly and systematically towards vein tip-lines.
9. Abrupt along-vein transitions in accretion increment thickness and number result from differential rates of mineral growth and indicate abrupt spatial variation in vein apertures.

Acknowledgements

Work for this paper was supported by a NERC/CASE award (GT4/88/GS/79) with Charter Consolidated PLC. We especially thank the hospitality and logistical support of Beralt Tin and Wolfram (Portugal) S.A.; particular thanks go to the general managers A. Correia de Sa, W. Berry and N. Devine and their staff, especially to M. Rotolo for his helpful advice and assistance. This manuscript was significantly improved by the editorial comments of Tom Blenkinsop and the constructive and incisive reviews of Stephen Cox and Guy Simpson.

References

Atkinson, B.K. (Ed.), 1987. Fracture Mechanics of Rock. Academic Press Geology Series, London.

Bahat, D., 1991. Tectonofractography. Springer-Verlag, Heidelberg.

Bahat, D., 1997. Mechanisms of dilatant en échelon crack formation in bedded chalk. Journal of Structural Geology 19, 1375–1392.

Barnett, J.A.M., Mortimer, J., Rippon, J.H., Walsh, J.J., Watterson, J., 1987. Displacement geometry in the volume containing a single normal fault. American Association of Petroleum Geologists Bulletin 71, 925–937.

Beach, A., 1975. The geometry of en-echelon vein arrays. Tectonophysics 28, 245–263.

Berner, R.A., 1980. Diagenetic chemical processes II: precipitation, dissolution and authigenic processes. In: Early Diagenesis: A Theoretical Approach. University Press, Princetown, pp. 90–126.

Boullier, A., Robert, F., 1992. Paleoseismic events recorded in Archean gold–quartz vein networks, Val d'Or, Abitibi, Quebec, Canada. Journal of Structural Geology 14, 161–179.

Burnham, W.C., 1985. Energy release in subvolcanic environments, implications for breccia formation. Economic Geology 80, 1515–1522.

Bussink, R.W., 1984. Geochemistry of the Panasqueira tungsten–tin deposit, Portugal. Geologica Ultraiectina 33, 170pp.

Cathles, L.M., Erendi, A.H.J., Barrie, T., 1997. How long can a hydrothermal system be sustained by a single intrusive event? Economic Geology 92, 766–771.

Childs, C., Watterson, J., Walsh, J.J., 1995. Fault overlap zones within developing normal fault systems. Journal of the Geological Society of London 152, 535–549.

Clark, M.B., Brantley, S.L., Fisher, D.M., 1995. Power-law vein-thickness distributions and positive feedback in vein growth. Geology 23, 975–978.

Cox, S.F., 1987. Antitaxial crack–seal vein microstructures and their relationship to displacement paths. Journal of Structural Geology 9, 779–788.

Cox, S.F., Etheridge, M.A., 1983. Crack seal fibre growth mechanisms and their significance in the development of oriented layer silicate microstructures. Tectonophysics 92, 147–170.

Cox, S.F., Etheridge, M.A., 1989. Coupled grain-scale dilatancy and mass transfer during deformation at high fluid pressures: examples from Mount Lyle, Tasmania. Journal of Structural Geology 11, 147–162.

Cox, S.F., Wall, V.J., Etheridge, M.A., Potter, T.F., 1991. Deformational and metamorphic processes in the formation of mesothermal vein-hosted gold deposits—examples from the Lachlan Fold Belt in Central; Victoria, Australia. Ore Geology Reviews 6, 391–423.

Cox, S.F., Sun, S.-S., Etheridge, M.A., Wall, V.J., Potter, T.F., 1995. Structural and geochemical controls on the development of the turbidite-hosted gold quartz vein deposits, Wattle Gully Mine, central Victoria, Australia. Economic Geology 90, 1722–1746.

de Caritat, P., 1990. Persistence of quartz disequilibrium in groundwater flows. Terra Nova 2, 53–59.

d'Orey, F.C., 1967. Tungsten–tin mineralization and paragenesis in the Panasqueira and Vale da Ermida mining districts, Portugal. Comunic. Serv. Geol. Portugal 52, 117–167.

Davison, I., 1995. Fault slip evolution determined from crack–seal veins in pull-aparts and their implications for general slip models. Journal of Structural Geology 17, 1025–1034.

Delaney, P.T., Pollard, D.D., 1981. Deformation of host-rocks and flow of magma during the growth of minette dykes and breccia bearing intrusions near Ship Rock, New Mexico, United States Geological Survey Professional Paper, 1202.

Derre, C., Lecolle, M., Roger, G., Tavares de Freitas Carvalho, J., 1986. Tectonics, magmatism, hydrothermalism and sets of flat joints locally filled by Sn–W, aplite–pegmatite and quartz veins, southeastern border of the Serra de Estrela granitic massif (Beira Baixa, Portugal). Ore Geology Reviews 1, 43–56.

Dickson, J.A.D., 1983. Graphical modelling of crystal aggregates and its relevance to cement diagnosis. Philosophical Transactions of the Royal Society of London A309, 465–502.

Fisher, D., Byrne, T., 1990. The character and distribution of mineralised fractures in the Kodiak Formation, Alaska: implications for fluid flow in underthrust sequences. Journal of Geophysical Research 95, 9069–9080.

Foxford, K.A. 1992. Fluid flow patterns during ore formation: con-

trols on mineralogical zoning at Minas da Panasqueira, Portugal. PhD Thesis, University of Manchester.

Foxford, K.A., Nicholson, R., Polya, D.A., 1991a. Textural evolution of W–Cu–Sn bearing hydrothermal quartz veins at Minas da Panasqueira, Portugal. Mineralogical Magazine 55, 435–445.

Foxford, K.A., Nicholson, R., Polya, D.A., 1991b. Evolution of wolframite-bearing quartz veins, Portugal. In: Pagel, M.P., Leroy, L.L. (Eds.), Source, Transport and Deposition of Metals. A.A. Balkema, pp. 447–450.

Foxford, K.A., Nicholson, R., Polya, D.A., Hebblethwaite, R.P.B., 1995. Conceptual methods for modelling systems of mineralised echelon veins: examples from southwest England and Portugal. Exploration and Mining Geology 4, 285–296.

Gillespie, P.A., Johnston, J.D., Loriga, E., McCaffrey, K.J.W., Walsh, J.J., Watterson, J., 1999. Influence of layering on vein systematics in line samples. In: McCaffrey, K.J.W., Lonegran, L., Wilkinson, J.J. (Eds.), Fractures, Fluid flow and Mineralisation, Geological Society Special Publication, 155, pp. 35–56.

Grady, D.E., Kipp, M.E., 1987. Dynamic rock fragmentation. In: Atkinson, B.K. (Ed.), Fracture Mechanics of Rock. Academic Press Geology Series, London, pp. 429–476.

Grigorev, D.P., 1965. Ontogeny of Minerals. Israel program for scientific translations, Jerusalem 260 pp.

Gross, M.R., Fischer, M.P., Engelder, T, Greenfield, R.J., 1995. Factors controlling joint spacing in interbedded sedimentary rocks: integrating numerical models with field observations from the Monterey Formation, USA. In: Ameen, M.S. (Ed.), Fractography: Fracture Topography as a Tool in Fracture Mechanics and Stress Analysis, Geological Society Special Publication, 92, pp. 215–233.

Halls, C., 1987. A mechanistic approach to the paragenetic interpretation of mineral lodes in Cornwall. Proceedings of the Ussher Society 6, 548–554.

Harwood, A., 1985. Tungsten–tin mineralisation at Chojlla in the Taquesi Batholith, Cordillera Real, Bolivia. In: Halls, C. (Ed.), High Heat Production (HHP) Granites, Hydrothermal Circulation and Ore Genesis. Institution of Mining and Metallurgy, London, pp. 549–561.

Hebblethwaite, R.P.B., Antão, A.M., 1982. A report on the study of dilation patterns within the Panasqueira orebody. Unpublished Beralt Tin and Wolfram (Portugal) S.A., unpublished report.

Henderson, J.R., Henderson, M.N., 1990. Crack–seal texture in bedding parallel, gold-bearing, columnar-quartz veins: evidence for fossil water sills. In: Sangster, A.L. (Ed.), Mineral Deposit Studies in Nova Scotia, Geological Survey of Canada Paper 90-8, 1, pp. 163–168.

Huggins, P.P., Watterson, J., Walsh, J.J., Childs, C., 1995. Relay zone geometry and displacement transfer between normal faults recorded in coal-mine plans. Journal of Structural Geology 17, 1741–1755.

Hull, D., 1993. Tilting cracks: the evolution of fracture surface topology in brittle solids. Journal of Fracture 62, 119–138.

Inverno, C., Ribeiro, M.L., 1980. Fracturacas e catejo nas Minas da argemlea (Fundão). Commincações dos Serviços Geologicos de Portugal 66, 185–194.

Jaeger, J.C., 1963. Extension failures in rocks subject to fluid pressure. Journal of Geophysical Research 68, 6066–6067.

Kelly, W.C., Rye, R.O., 1979. Geologic, fluid inclusion and stable isotope studies of the tin–tungsten deposits of Panasqueira, Portugal. Economic Geology 74, 1721–1822.

Lorentz, J.C., Teufel, L.W., Warpinski, N.R., 1991. Regional fractures I: a mechanism for the formation of regional fractures at depth in flat-lying reservoirs. American Association of Petroleum Geologists Bulletin 75, 1714–1737.

Lawn, B.R., Wilshaw, T.R., 1975. Fracture of Brittle Solids. Cambridge University Press, New York.

Main, I., Meredith, P.G., Sammonds, P.R., Jones, C., 1990. Influence of fractal flaw distribution on rock deformation in the brittle field. In: Knipe, R.J., Rutter, E.H. (Eds.), Deformation Mechanisms, Rheology and Tectonics, Geological Society Special Publication, 54, pp. 81–96.

Mello Mendes, F., Correia De Sa, A., Ferreira, E., Silva, J., 1987. In: The Geomechanics of Panasqueira Mine, Portugal. 6th Congress of the International Society for Rock Mechanics, Montreal, pp. 1145–1152.

Nicol, A., Watterson, J., Walsh, J.J., Childs, C., 1996. The shapes, major axis orientations and displacement patterns of fault surfaces. Journal of Structural Geology 18, 235–248.

Nicholson, R., 1991. Vein morphology, host-rock deformation and the origin of the fabrics of échelon mineral veins. Journal of Structural Geology 13, 635–641.

Nicholson, R., Pollard, D.D., 1985. Dilation and linkage of échelon cracks. Journal of Structural Geology 7, 583–590.

Nicholson, R., Ejiofor, I., 1987. The three-dimensional morphology of arrays of echelon and sigmoidal, mineral-filled fractures: data from Cornwall. Journal of the Geological Society of London 144, 79–83.

Olson, J.E., 1993. Joint pattern development: effects of subcritical crack growth and mechanical crack interaction. Journal of Geophysical Research 98, 12251–12265.

Olson, J.E., Pollard, D.D., 1989. Inferring palaeostress from natural fracture patterns: a new method. Geology 17, 345–348.

Olson, J.E., Pollard, D.D., 1991. The initiation and growth of en-échelon veins. Journal of Structural Geology 13, 595–608.

Peacock, D.C.P., 1991. A comparison between the displacement geometries of veins and normal faults at Kilve, Somerset. Proceedings of the Ussher Society 7, 363–367.

Pollard, D.D., 1987. Elementary fracture mechanics applied to the structural interpretation of dikes. In: Halls, H.C., Fahrig, W.F. (Eds.), Mafic Dike Swarms, Geological Association of Canada Special Publication, 34, pp. 5–24.

Pollard, D.D., Aydin, A., 1988. Progress in understanding jointing over the past century. Geological Society of America Bulletin 100, 1181–1204.

Pollard, D.D., Muller, D.H., Dockstader, D.R., 1975. The form and growth of fingered sheet intrusions. Geological Society of America Bulletin 86, 351–363.

Pollard, D.D., Segal, P., 1987. Theoretical displacements and stresses near fractures in rocks: with applications to faults, joints, dikes and solution surfaces. In: Atkinson, B.K. (Ed.), Fracture Mechanics of Rock. Academic Press Geology Series, London, pp. 277–350.

Pollard, D.D., Segal, P., Delaney, P.T., 1982. Formation and interpretation of dilatant echelon cracks. Geological Society of America Bulletin 93, 1291–1303.

Polya, D.A., 1988. Efficiency of hydrothermal ore formation and the Panasqueira W–Cu(Ag)–Sn vein deposit. Nature 333, 838–841.

Polya, D.A., 1989. Chemistry of the mainstage ore-forming fluids of the Panasqueira W–Cu(Ag)–Sn deposit, Portugal: implications for models of ore genesis. Economic Geology 84, 1134–1152.

Polya, D.A., Foxford, K.A., Stuart, F., Boyce, A., Fallick, A.E., 2000. Evolution and paragenetic context of low δD hydrothermal fluids from the Panasqueira W–Sn deposit, Portugal: new evidence from microthermometric, stable isotope, noble gas and halogen analyses of primary fluid inclusions. Geochimica Cosmochimica Acta, in press.

Price, N.J., Cosgrove, J.W., 1990. Analysis of Geological Structures. Cambridge University Press, 502 pp.

Ramsay, J.G., 1980. The crack–seal mechanism of rock deformation. Nature 284, 135–139.

Ramsay, J.G., Huber, M.I., 1983. The Techniques of Modern Structural Geology, Volumes 1 and 2. Academic Press, London.

Renshaw, C.E., Pollard, D.D., 1994. Are large differential stresses

required for straight fracture propagation paths? Journal of Structural Geology 16, 817–822.

Roberts, S., Sanderson, D.J., Gumiel, P., 1999. Fractal analysis and percolation properties of veins. In: McCaffrey, K.J.W., Lonegran, L., Wilkinson, J.J. (Eds.), Fractures, Fluid Flow and Mineralisation, Geological Society Special Publication, 155, pp. 7–16.

Rodrigues, A.P., 1985. Reservas dos Niveis 1 e 2. Unpublished report, Beralt Tin and Wolfram (Portugal) SA.

Rogers, R.D., Bird, D.K., 1987. Fracture propagation associated with dike emplacement in the Skeargaard intrusion, east Greenland. Journal of Structural Geology 9, 71–86.

Sanderson, D.J., Roberts, S., Gumiel, P., 1994. A fractal relationship between vein thickness and ore grade in drill core from La Codosera, Spain. Economic Geology 89, 63–71.

Secor, D.T., 1965. Role of fluid pressure in jointing. American Journal of Science 263, 633–646.

Segal, P., Pollard, D.D., 1983. Joint formation in granitic rock of the Siera Nevada. Geological Society of America Bulletin 94, 563–575.

Sibson, R.H., 1981. Controls on low-stress hydrofracture in thrust, wrench and normal fault terrains. Nature 289, 665–667.

Sibson, R.H., 1990. Conditions for fault valve behaviour. In: Knipe, R.J., Rutter, E.H. (Eds.), Deformation Mechanisms, Rheology and Tectonics, Geological Society Special Publication, 54, pp. 15–28.

Sibson, R.H., 1994. Crustal Stress, faulting and fluid flow. In: Parnell, J. (Ed.), Geofluids: Origin, Migration and Evolution of Fluids in Sedimentary Basins, Geological Society Special Publication, 78, pp. 69–84.

Sibson, R.H., Robert, F., Poulson, K.H., 1988. High angle reverse faults, fluid pressure cycling and mesothermal gold–quartz deposits. Geology 16, 551–555.

Sillitoe, R.H., 1985. Ore-related breccias in volcanoplutonic arcs. Economic Geology 80, 1467–1514.

Smith, A., 1979. Mining at Panasqueira mine, Portugal. Transactions of the Institute of Mining and Metallurgy 88, A108–A115.

Snee, L.W., Sutter, J.F., Kelly, W.C., 1988. Thermochronology of economic deposits: dating the stages of mineralisation at Panasqueira, Portugal, by high precision $^{40}Ar/^{39}Ar$ age spectrum techniques on muscovite. Economic Geology 83, 335–354.

Thadeu, D., 1951. Geologia do couto mineiro da Panasqueira. Comunic. Serv. Geol. Portugal 32, 5–64.

Urai, J.L., Williams, P.F., van Roermund, H.L.M., 1991. Kinematics of crystal growth in syntectonic fibrous veins. Journal of Structural Geology 13, 823–836.

Vermilye, J.M., Scholz, C.H., 1995. Relation between vein length and aperture. Journal of Structural Geology 17, 423–434.

Walsh, J.J., Watterson, J., 1991. Geometric and kinematic coherence and scale effects in normal fault systems. In: Roberts, A.M., Yielding, G., Freeman, B. (Eds.), The Geometry of Normal Faults, 56. Geological Society of London Special Publication, pp. 193–203.

Williams, C.T.P., 1985. Ore estimation and mine planning at Panasqueira. Unpublished Ph.D. thesis, Royal School of Mines, University of London.

Wu, H., Pollard, D.D., 1993. Effect of strain rate on a set of fractures. International Journal of Rock Mechanics. Mining Science and Geomechanics Abstracts 30, 869–872.